51

A SURFACE ALBEDO MAP OF PLUTO BASED ON PHOTOMETRY OF MUTUAL EVENTS

by

Eliot F. Young

A.B., Amherst College, (1984)

S.M., Massachusetts Institute of Technology, (1987)

SUBMITTED IN PARTIAL FULFILLMENT
OF THE REQUIREMENTS FOR
THE DEGREE OF

MASTER OF SCIENCE
IN EARTH, ATMOSPHERIC AND PLANETARY SCIENCES

at the

MASSACHUSETTS INSTITUTE OF TECHNOLOGY
September 1990

© Massachusetts Institute of Technology 1990

Signature of the Author_____
Department of Earth, Atmospheric and Planetary Science
September 10, 1990

Certified by_____
Prof. Richard P. Binzel
Thesis Supervisor
Department of Earth, Atmospheric and Planetary Sciences

Accepted by_____
Prof. Thomas Jordan
Chairman, Department Graduate Committee

MASSACHUSETTS INSTITUTE OF TECHNOLOGY
WITHDRAWN
OCT 23 1990
FROM
MIT LIBRARIES

Acknowledgments

I would like to thank Rick Binzel. He has been very supportive throughout this project, and I hope someday I can return the favor. I must also thank Leslie Young, who helped figure out most of the more difficult problems in this thesis, and listened to me explain the entire thing when she had better things to do. My appreciation to my patient officemates, Amanda, Steve, and Shui. And, of course, I thank my parents.

Table of Contents

Abstract

Photometric observations of Pluto-Charon mutual events obtained at the University of Texas McDonald Observatory from 1985 through 1990 enable us to construct an albedo map for the Charon-facing hemisphere of Pluto. The surface of Pluto is divided into eleven contiguous panels. We calculate an average albedo for each panel based on the change in observed brightness when that panel is covered or uncovered by Charon. A least squares fitting algorithm is used to find the panel albedos that best match the observed lightcurves. To monitor the uniqueness of the solution, a singular value decomposition algorithm is used in implementing the least squares fit. The eleven panel map shows a large, bright region over the south pole, but a similar cap is not observed over the north pole.

Chapter One

Introduction

In August of 1990 the spacecraft *Magellan* achieved orbit around Venus and subsequently returned unprecedentedly high resolution radar mapping images of the Venusian surface. A few months earlier Voyager II successfully imaged Neptune and Triton. This leaves the Pluto-Charon system as the only major planetary system which has not been visited by spacecraft and for which there exist no high resolution pictures.

In the absence of spacecraft observations, how can we image the surfaces of Pluto and Charon? Consider that Pluto's radius is only two thirds that of the Moon's, and its closest approach to the Earth is 28.8 A.U. Pluto's disk subtends at most 0.1 arcsec, and the maximum Charon-Pluto separation is approximately 0.9 arcsec. What would seem to be an impossible problem for Earth-based observers has become possible through a unique geometry. From 1985 through 1990 the plane of Charon's orbit has been such that part of Pluto has been eclipsed by Charon every time Charon passes in front of Pluto, which occurs every 6.4 days. These events allow us to build up a map of Pluto's surface (a procedure which is described in detail in the next section).

Obviously the surface features of Pluto are intrinsically interesting, but even more interesting are the ongoing processes on Pluto which are suggested by clues in the surface map. Specifically, a surface map allows us to discuss the following questions:

Interaction between the surface and the atmosphere:

- Is there evidence for "atmospheric laundering" (periodic separation of chemical compounds on Pluto's surface by sublimation and recondensation)?
- Is there evidence for a transient atmosphere? How does the atmospheric composition change as a function of Pluto's orbital position?
- How important are meteorological effects? Can Pluto sustain large temperature differences over its relatively small surface? If various regions on Pluto have different energy absorption rates (because of different albedos, for example), does the atmosphere equilibrate fast enough to prevent large scale "hot" and "cold" behavior, such as frost condensation only over the "cold" regions?

Age of the surface:

- Is all of Pluto's surface young? What is the relationship between age and albedo?
- Would any impact features be visible on Pluto? If there is continuous planetary resurfacing, is it deep enough to obliterate impact features, and on what timescale?

Depth of surface:

- How deep is the visible layer on Pluto's surface?
- What is the total volatile reservoir on Pluto? How long will this reservoir last? How much has been lost?

These questions motivate the surface albedo map of Pluto. The immediate goals of this paper are (a) to show

the feasibility of the map making scheme, (b) to make a preliminary map of Pluto based on several mutual event lightcurves, and (c) to interpret new information which the map might yield.

Pluto-Charon Mutual Events

When Charon was discovered in 1978 the plane of its orbit was nearly parallel to the line of sight from the Earth. By 1985 the plane of Charon's orbit was such that occultations of Pluto's north pole by Charon were observed [Binzel, R.P. et al. 1985]. As Pluto's heliocentric motion continued to change the apparent orientation of Charon's orbit, Charon's impact parameter moved from northern latitudes to southern ones. The goal of this paper is to construct an albedo map of Pluto based on six well observed mutual occultation events that occurred between Pluto and Charon from 1985 through 1990.

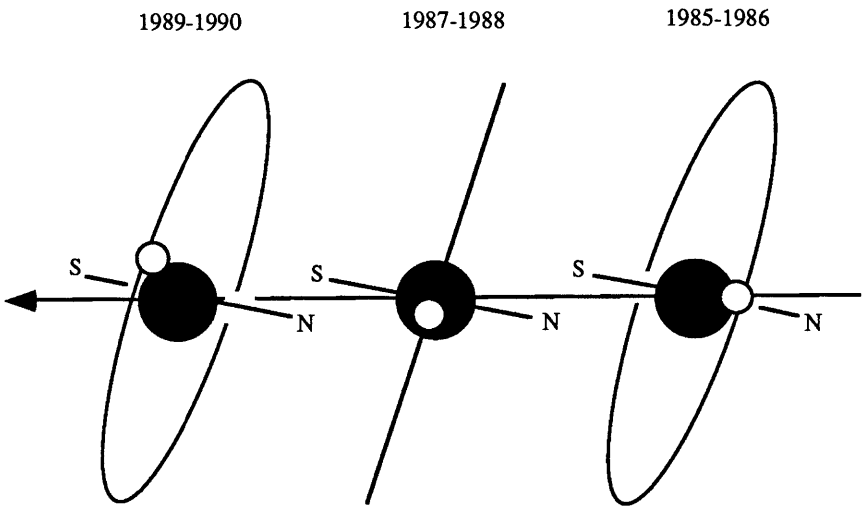

Figure 1.1
In the early mutual events (in 1985 and 1986) Charon transited across Pluto's North pole. Pluto's heliocentric motion moves the band of coverage from north to south, until, in 1989 and 1990, only the southern polar latitudes are transited. Up is north, referenced to the Earth's equator. Pluto's north pole is defined by the right hand rule applied to Pluto's spin axis.

As shown in Figure 1.1, Charon has progessively transited northern, equatorial, and southern regions over the period 1985 through 1990. Photometric observations of the mutual events over the last six years thus contain complete coverage of Pluto's Charon-facing hemisphere. Mutual events will occur again in 2109, when Pluto is 180° from its current position about the Sun.

How do we construct a surface map of Pluto from the frequent mutual occultations? During an occultation the brightness of the Pluto-Charon system diminishes because some of the reflecting area of Pluto is obscured by its satellite. If both objects are uniform, gray disks, then the decrease in brightness would correspond exactly to the fractional area being covered. If, however, the covered region is a little brighter than average, then the decrease in brightness would be greater than the relative change in area. A smaller-than-expected decrease in brightness would

be observed when dark regions are obscured. By keeping track of the changes in brightness that occur as various parts of Pluto are covered and uncovered, we can piece together an albedo map for one hemisphere of Pluto.

Why just one hemisphere? Pluto and Charon are in mutually synchronous orbits. Since the rotations of both bodies are tidally locked (as is the case for the Earth's moon), Pluto and Charon always present the same face to each other. Only the Charon-facing hemisphere of Pluto is ever transited by Charon. Although mutual event lightcurves are limited to the Charon-facing half of Pluto, the repeated transits yield unusually good coverage of that one hemisphere.

The separation between Pluto and Charon is roughly 19,640 km, currently best determined from speckle interferometry [Beletic, J. W. et al. 1989]. Even at perihelion, Pluto and Charon subtend an angle of only 0.9 arcsec at maximum elongation. Accurate relative positions of Pluto and Charon cannot be determined from even the best ground-based optical telescopes. We know an event is in progress from photometric measurements of the short-term decrease in the brightness of the Pluto-Charon system. Beletic et al. have used the timing of the mutual events to perform a least squares fit for Charon's orbital elements [Beletic, J. W. et al. 1989]. These have been refined by Tholen and Buie [Tholen, D.J., and Buie, M.W. 1989].

Semimajor axis = 19640 ±320 km
Eccentricity = 0.00009 ± 0.00038
Inclination = 98.3 ± 1.3°
Ascending node = 222.37 ±0.07°[1]
Argument of periapses = 290 ± 180°[2]
Mean anomaly = 259.90 ±0.15°[3]
Epoch = JDE 2,446,600.5 = 19 June 1986
Radius of Pluto = 1142 ± 9 km
Radius of Charon = 596 ± 17 km

Table 1.1 Important orbital parameters for the Pluto-Charon system.

With these orbital parameters we can calculate the positions of Pluto, Charon, the Earth and the Sun at a given time. We can recreate the viewing geometry of Pluto and Charon for every one of the points on a lightcurve. The model of Pluto and Charon predicts a magnitude for that point on the lightcurve, depending on how much of Pluto's disk is covered and on the albedo of the covered region. The measured lightcurve intensity can therefore be used to determine the surface brightness of the covered region.

1. Referred to the mean equator and equinox of 1950.0.
2. Referred to the mean equator and equinox of 1950.0.
3. Measured from the ascending node.

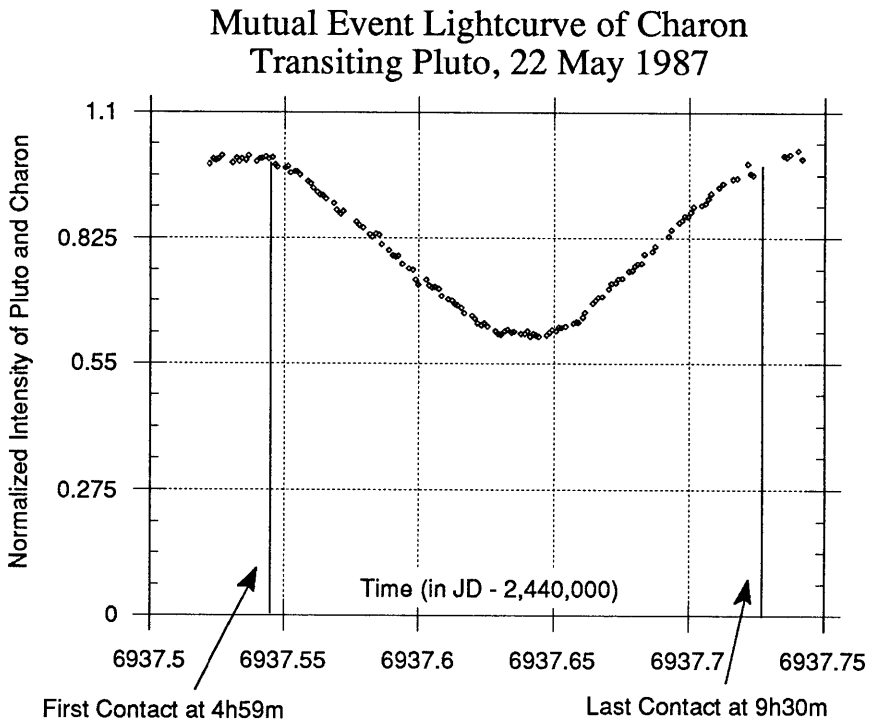

Figure 1.2 This occultation of Pluto by Charon and its shadow lasted 4.5 hours. The depth is about 61% of the baseline intensity, which is roughly the fractional disk area of Pluto and Charon that is still exposed at mid-event.

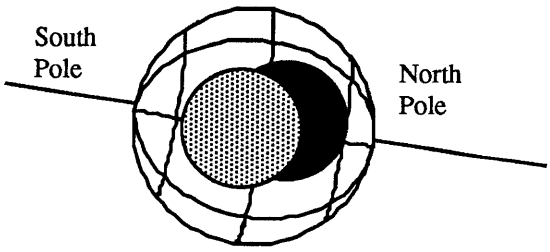

Figure 1.3 A somewhat artificial example of how Pluto might be divided into panels. In this case Pluto is split into twelve panels, four of which are shown to be partially covered by Charon or its shadow.

Our model of Pluto predicts a brightness during an occultation that depends on the brightness and the exposed area of each panel. The least squares fitting routine finds the panel albedos that best match the observed lightcurves. How do we combine the different overlapping regions, each with its own average albedo, into a single surface map? We divide the surface of Pluto into panels. The brightness of each panel is a parameter which is fitted by the least squares algorithm.

Chapter Two

A Brief Review of Pluto and Plutonian Surface Maps

The Size of Pluto

Pluto's existence was first proposed to account for anomalies in Neptune's orbit. Initial estimates for the mass of the unknown planet were in the neighborhood of six earth masses [Hoyt, W.G. 1980][4]. After Pluto was discovered by Clyde Tombaugh, an orbit was fitted to its observed positions, and Pluto's heliocentric distance was determined. At that point Pluto's size could be estimated from its luminosity, its distance, and some guess as to its reflectivity.

Precise timing of occultations is an accurate way of determining planet radii, and the Pluto-Charon transits provide an occultation every 6.38 days. Unfortunately, all of the length measurements (such as Pluto's and Charon's radii) depend on the separation of Pluto and Charon, which currently is best determined from speckle interferometry [Beletic, J. W. et al. 1989]. A stellar occultation by Pluto on June 9, 1988 yields a set of lightcurves which may be the best direct measurements of Pluto's radius. The stellar occultation was also the first direct detection of Pluto's atmosphere. The atmosphere was not modeled in the estimates of Pluto's radius that were based on the mutual events. The stellar occultations provide at best an upper limit on the solid radius of Pluto: it is 1143 ± 20 km, the deepest level probed by the occultation [J.L. Elliot et al 1989].

Methane Frost and Pluto's Atmosphere

Pluto's high albedo, combined with spectrographic identification of methane on Pluto, strongly suggests recently deposited methane frost on Pluto's surface. The detection of an atmosphere on Pluto [J.L. Elliot et al 1989] provides a mechanism for the continuous formation of frost layers. A paper by Stern, Trafton and Gladstone [S. A. Stern et al 1988] covers this topic in depth. Pluto's atmosphere is a transient phenomenon, and its methane component will freeze out as Pluto recedes from the Sun. How recent is Pluto's frost layer? Stern et al. calculate that a frost layer of methane would be polymerized by solar UV radiation and galactic cosmic rays to form an optically thick layer of darker material (100 μm) in 100,000 years. Their main conclusions:

> Summarizing, we first conclude that in order for Pluto to remain bright, recently exposed volatile frosts must be present on the surface. Second, we conclude that the bright surface results from an "atmospheric laundering" process in which volatiles are cleansed of dark material by their annual sublimation into and freezeout from the atmosphere. Finally, we conclude that CH_4 losses to escape and photolysis may be made up by thermally driven sublimation across the photolysis layer.[S. A. Stern et al 1988].

4. One of Percival Lowell's predictions for 'Planet X' was a body six times the mass of the Earth, with orbital parameters surprisingly close to Pluto's actual values. Lowell was probably motivated to pick such a large mass to account for (a) supposed residuals in the motion of Neptune, and (b) comets, which were apparently perturbed from their orbits in the distant solar system by a massive object.

Previous Maps of Pluto

It is possible to construct a surface map of a rotating body without the aid of occultation lightcurves, relying instead solely upon rotation lightcurves. This technique has many shortcomings, however. If the axis of rotation is not perpendicular to the observer's line of sight, then much of the rotating body may never come into view, and the lightcurve may show almost no variation with rotation. Even if the axis of rotation is perpendicular to the line of sight (as is currently the case with Pluto), the rotation lightcurves do not produce a unique surface map, as Wild [Wild, W. J. 1989] points out. For example, the following two albedo distributions could both be solutions to the same rotation lightcurve.

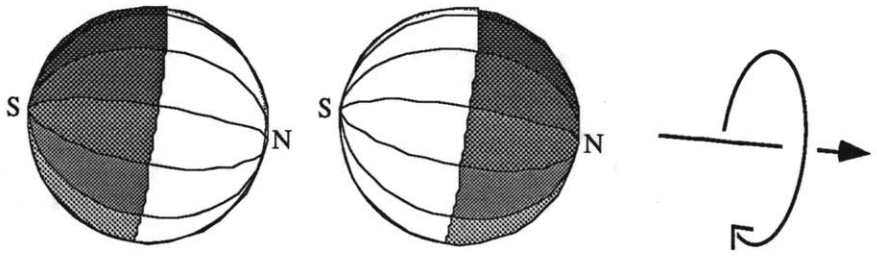

Figure 2.1 An example of two surface albedo distributions which cannot be distinguished from rotational lightcurves. Even though these two surface distributions are mirror images of each other in longitude, the rotation lightcurves produced by the pair would be identical.

Variations in the overall brightness of the body occur as sections disappear and reappear around the limb. In Pluto's case, the limb provides high resolution in longitude but almost none in latitude[5]. Nevertheless, several surface maps were developed before the mutual event data were available.

The Two-Spot Model

The two-spot model attempts to fit the rotation lightcurves with two dark, circular spots on Pluto. The free parameters in the model are the two spot sizes, the ratio of the spotted albedo to the unspotted albedo, the single central latitude of the two spots, and the separation in longitude of the two spots. The author of the two-spot model [Marcialis, R.L. 1983] points out that while spot models have historically been used to study variable stars, they are better suited to the study of solid bodies. The two-spot model circumvents the problem of nonunique solutions associated with inverting the rotation lightcurves by assuming a specific model for Pluto's surface *a priori*. By including data sets from as early as 1953, Marcialis can get some information on the latitude variation on Pluto. The results of the least squares fit to the rotation lightcurves yields the following parameters.

5. Plutonian lightcurves have been measured for a long time, and there has been a slow but steady increase in the amplitude of the variation in these lightcurves as well as an overall dimming of the average albedo. This trend can be attributed to the changing orientation of Pluto from a pole-on view to its current sideways position. Some resolution in latitude may be inferred from these trends.

Big Spot Radius	46°
Small Spot Radius	28°
Albedo Ratio	1/2
Central Spot Latitude	23° S.
Spot Separation in Longitude	134°

Table 2.1 Provisional working two-spot model [Marcialis, R.L. 1983].

A projection of the provisional two-spot model as described above is shown in Figure 2.2.

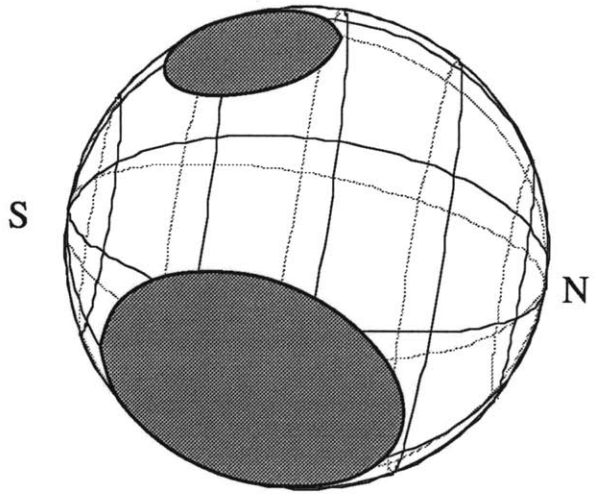

Figure 2.2 A graphic of the two-spot model as it would appear in 1985.

The MAX and SHELF Models

The MAX and SHELF models [Buie, M.W. and Tholen, D.J. 1988] are essentially four-spot models (as opposed to two-spot models), with two of the spots located over the poles, and two other spots located over mid-equatorial latitudes. There are five parameters associated with each spot: the spot albedo, an average phase function coefficient, the spot diameter, and the latitude and longitude of the spot center. In addition, the model fits for the average albedo and phase coefficient for Charon and Pluto's background. The total number of free parameters would be 24, except that the spot on the south pole is defined to be centered at the south pole, thereby reducing the number of parameters by two. Both the MAX and the SHELF models assume that the polar spots are brighter than the background. The two mid-latitude spots are both darker than the background in the MAX model, whereas the SHELF model has one darker, one brighter[6]. In the tables below w is the single scattering albedo and $P(0)$ is the average particle phase

6. Buie and Tholen also tried a MIN model, which initially had two brighter mid-latitude spots. The MIN, MAX, and SHELF models all served as different starting points for a simplex algorithm, an algorithm which modifies free parameters to minimize a function, such as the sum of the squared residuals. The MIN model parameters "quickly migrated towards those for SHELF." Thus [Buie, M.W. and Tholen, D.J. 1988] only present the MAX and SHELF models.

function for 180° scattering angle.

	Radius (km)	*w*	*P(0)*
Pluto (unspotted)	1162.0	0.776	2.1
Charon (global)	620.7	0.863	1.

Spot	*Latitude*	*Longitude*	*Radius*	*w*	*P(0)*
#1	-1.9	110.1	30.6	0.406	0.4
#2	-23.0	195.2	14.8	0.971	2.9
#3	81.4	195.6	59.4	0.999	2.2
#4	*south pole*		44.2	1.000	1.5

Table 2.2 Spot model parameters for SHELF, from Table III of [Buie, M.W. and Tholen, D.J. 1988].

	Radius (km)	*w*	*P(0)*
Pluto (unspotted)	1162.0	0.789	2.4
Charon (global)	620.7	0.863	1.

Spot	*Latitude*	*Longitude*	*Radius*	*w*	*P(0)*
#1	-13.9	99.1	31.0	0.064	2.6
#2	-25.9	315.7	17.4	0.142	1.4
#3	79.6	213.4	62.4	1.000	1.3
#4	*south pole*		45.3	1.000	1.5

Table 2.3 Spot model parameters for MAX, from Table IV of [Buie, M.W. and Tholen, D.J. 1988].

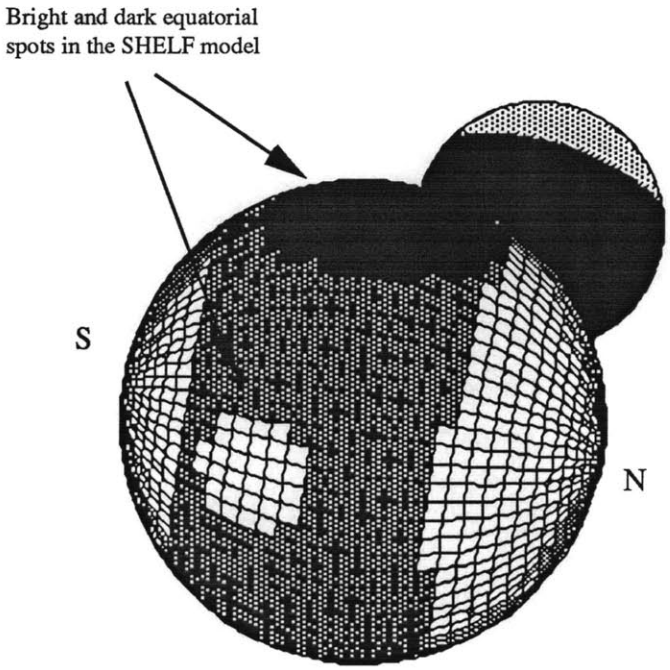

Figure 2.3 The SHELF model, Jan 23, 1988 (with Charon emerging from eclipse). adapted from Figure 9 from [Buie, M.W. and Tholen, D.J. 1988].

The total χ^2 value for the MAX model is 1844, for the SHELF model it is 1768. The quality of the fit is nearly the same for both models, yet the resulting surfaces are different. Clearly the mutual event data would help to distinguish the various rotation lightcurve solutions. Buie and Tholen compared early mutual event lightcurves to predictions of both the MAX and SHELF models, and found that the MAX model is inconsistent with the observations, while the SHELF model matched the mutual event lightcurves "quite closely." Since the SHELF model is the most recent published model of Pluto's surface, we compare it to our own model in chapter 3.

Previous Mutual Event Modeling

Dunbar and Tedesco [Dunbar, R.S. and Tedesco, E.F. 1986] have made a simple model which includes as parameters Pluto's and Charon's average albedos and their radii. The three circle approximation (Charon, Pluto, and Charon's shadow) is a useful approach which we have adopted to project the Pluto-Charon system onto the projection plane. The authors have also solved the problem of calculating the common area overlapped by three circles, a problem which we solved somewhat less elegantly with a discrete grid (see Appendix D, equation D.2).

Current Work

We are aware of two projects currently working on the construction of surface maps from mutual event data. [Buie, M.W. et al. 1989] have constructed a methane map of Pluto's surface from mutual event observations through Johnson K filters (which pass light in a strong absorption regime of methane). These observations were made at the

IRTF. [Horne, K., Buie, M., and Tholen, D.J. 1988] are in the process of fitting a map of Pluto to mutual event lightcurves using a maximum entropy method to bypass the problem of how to divide the surface of Pluto into discrete panels. We do not know whether this method can gauge the uniqueness of its solution.

Chapter Three

The Eleven Panel Map

Using six mutual event lightcurves, we decided to break up the surface into eleven panels. These eleven panels split the Charon-facing hemisphere into four bands of latitude. The singular value decomposition implementation of the least squares solution [Appendix B] was used to find the relative intensities of each panel. These are scaled so that the combined output of all the panels equals the average geometric albedo of Pluto's Charon-facing hemisphere. Figure 3.2 is a graphic representation of the least squares solution for the eleven panel model. The sub-Charon longitude defines the prime meridian (line of zero longitude) on Pluto[7].

What is the rationale for using an eleven panel map? Why not use a 400 panel map? Since we suspected the existence of polar caps on Pluto, resolution in latitude was our primary objective. Splitting Pluto's disk into three bands of latitude left us with too crude a map, and five bands resulted in polar panels that were too small. Too small was operationally defined by (a) a singular value of zero associated with the panel, or (b) a panel whose formal error from the least squares fit was over 10% of the average Pluto albedo of 0.5. Once we had decided on four bands of latitude (delineating Pluto at the equator and at $\pm$ 60°), the next step was to break each band into panels along lines of longitude. The polar bands were both split into two panels; three panels would have been 'too small.' The resolution of the mid-latitude bands is limited by the amount of coverage by Charon transits. Figure 3.1 (below) shows that the mid-northern band is covered by one more transit than the mid-southern latitude. We were able to divide the mid-northern latitude into four panels (labeled **C**, **D**, **E** and **F**). The mid-southern band, with somewhat sparser coverage, could be divided into three panels (**G**, **H**, and **I**).

7. [Buie, M.W. and Tholen, D.J. 1988] use the same definition for Pluto's prime meridian.

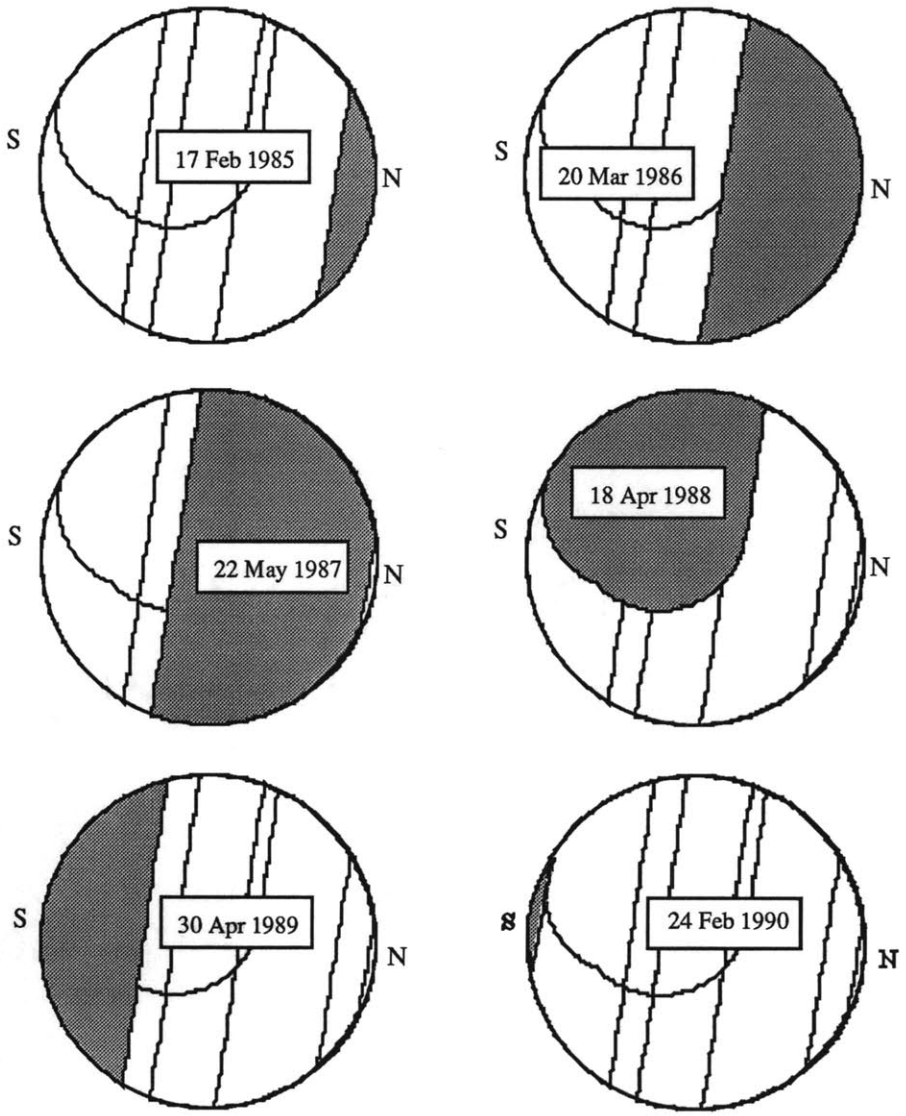

Figure 3.1 Coverage of Pluto's disk by Charon transits. The shaded portion of each disk indicates the area covered by that particular transit. The borders of each transit are drawn on all five disks. The 18 Apr. 88 event was interrupted by astronomical twilight, and thus stops short of a complete transit.

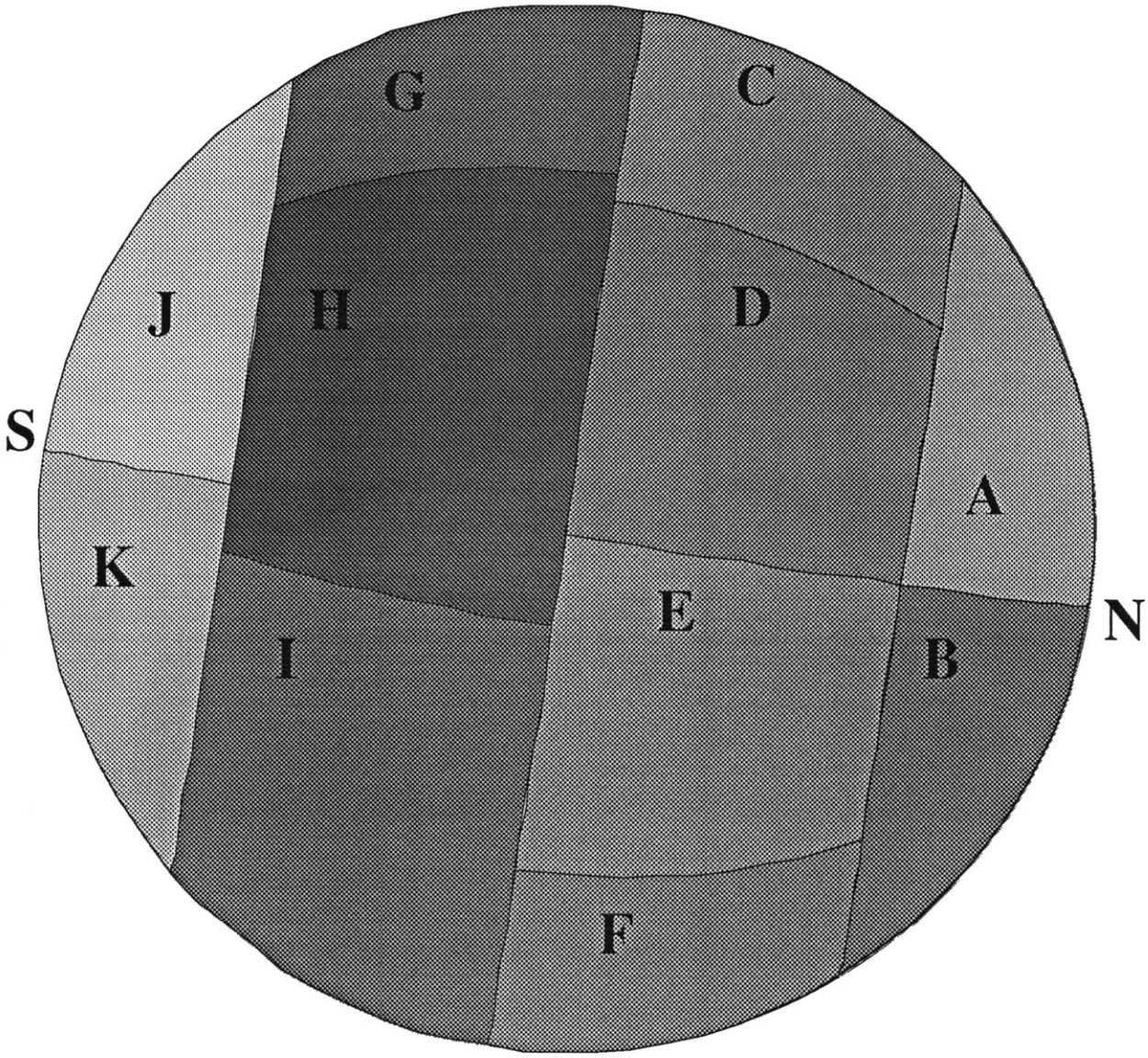

Geometric Albedos

A.....0.69 ±0.041	G.....0.33 ±0.030
B.....0.43 ±0.045	H.....0.25 ±0.023
C.....0.57 ±0.023	I.....0.37 ±0.027
D.....0.50 ±0.022	J.....0.87 ±0.034
E.....0.58 ±0.022	K.....0.81 ±0.043
F.....0.53 ±0.028	

Figure 3.2 The least squares solution to the eleven panel map. Gray scales are used to illustrate the geometric albedos for each panel. Scaling is such that white = 1, black = 0. (Recall that geometric albedos may be greater than one.) Bear in mind that the shape of each panel is an artifact of (a) the large size of the panels, and (b) the nature of the coverage by Charon, which encouraged us to delineate panel boundaries along lines of latitude and longitude.

The quoted errors in Figure 3.2 are the formal errors of the least squares problem. Specifically, the error in the i^{th} parameter is

$$\sigma_i = \sqrt{\frac{\chi^2}{n - m} \mathrm{Cov}[i, i]}$$

Equation 3.1 Estimate of one standard deviation in a least squares solution.

where n is the number of observations, m is the number of parameters, χ^2 is the sum of the squared weighted residuals, and Cov[i, i] is the i^{th} diagonal element of the covariance matrix. The covariance matrix for the eleven panel map is

	A	B	C	D	E	F	G	H	I	J	K
1	0.00167	-0.0014	-0.0003	-0.0006	0.00028	0.00042	9.1E-05	0.00019	-0.0002	-0.0003	0.00034
2	-0.0014	0.00207	0.00013	0.00053	-0.0006	-0.0005	4.5E-05	-0.0002	9.6E-05	0.00045	-0.0001
3	-0.0003	0.00013	0.00052	-0.0001	0.00011	-0.0001	-0.0004	4.7E-05	-2E-05	3.5E-05	4.9E-05
4	-0.0006	0.00053	-0.0001	0.00051	-0.0003	4.2E-05	0.00023	-0.0003	5.4E-05	0.0003	-0.0001
5	0.00028	-0.0006	0.00011	-0.0003	0.00049	-6E-05	-0.0001	0.00018	-0.0001	-0.0003	0.00019
6	0.00042	-0.0005	-0.0001	4.2E-05	-6E-05	0.0008	0.00027	-1E-04	-0.0004	3.1E-05	0.00047
7	9.1E-05	4.5E-05	-0.0004	0.00023	-0.0001	0.00027	0.00091	-0.0004	-7E-05	-5E-06	0.00023
8	0.00019	-0.0002	4.7E-05	-0.0003	0.00018	-1E-04	-0.0004	0.00054	-0.0002	-0.0005	0.00023
9	-0.0002	9.6E-05	-2E-05	5.4E-05	-0.0001	-0.0004	-7E-05	-0.0002	0.00075	0.00031	-0.0011
10	-0.0003	0.00045	3.5E-05	0.0003	-0.0003	3.1E-05	-5E-06	-0.0005	0.00031	0.00121	-0.0008
11	0.00034	-0.0001	4.9E-05	-0.0001	0.00019	0.00047	0.00023	0.00023	-0.0011	-0.0008	0.0019

Table 3.1. The covariance matrix from the eleven panel least squares fit. The row numbers **1** through **11** refer to panels **A** through **K**.

The sum of squared residuals for this fit is 0.049662. χ^2, the sum of weighted residuals, is 1916.22. Since we fit eleven parameters using 483 observations, the χ^2 per degree of freedom is 3.98.

$$\chi^2 = \left(\frac{y_i - y'_i}{\sigma_i}\right)^2$$

Equation 3.2 Definition of χ^2, where σ_i is the standard deviation of the i^{th} measurement, y_i is the the i^{th} measurement, and y'_i is the the i^{th} point predicted by the model.

Errors in the Physical Parameters

The formal errors of the least squares fit are a useful estimate of the quality of the fit. They have the disadvantage, however, of being scaled by χ^2, which depends only on the difference between the model predictions and the observed lightcurves, as opposed to the precision of the raw measurements. Ideally we would propagate the measurement errors to get estimates of the errors in the fitted parameters, but the irregular shape of the panels and the

complicated geometry involved in the exposure of Pluto's disk make a straightforward calculation of propagated errors impossible. We concentrate instead on estimating the model's sensitivity to errors in three of the most crucial model parameters: Pluto's radius, Charon's radius, and Charon's semimajor axis. The separation between Pluto and Charon that we used in this paper is based on speckle interferometry [Beletic, J. W. et al. 1989]. Pluto's and Charon's radii, determined from the timing of mutual events, both scale linearly with Charon's semimajor axis. To gauge the effect that an error in Pluto's or Charon's radii, or the semimajor axis would have, we varied each of those three parameters (while holding the other two constant) and solved for the panel albedos.

Charon Size Survey

	Rc = 570 km		Rc = 585 km		Rc = 600 km		Rc = 615 km		Rc = 630 km	
A	0.54	±0.04	0.55	±0.04	0.58	±0.04	0.62	±0.04	0.68	±0.04
B	0.37	±0.05	0.37	±0.04	0.35	±0.04	0.34	±0.04	0.33	±0.04
C	0.53	±0.02	0.54	±0.02	0.55	±0.02	0.55	±0.02	0.55	±0.02
D	0.62	±0.02	0.59	±0.02	0.56	±0.02	0.52	±0.02	0.47	±0.02
E	0.66	±0.02	0.63	±0.02	0.59	±0.02	0.56	±0.02	0.52	±0.02
F	0.58	±0.03	0.53	±0.03	0.49	±0.02	0.46	±0.02	0.43	±0.03
G	0.36	±0.03	0.35	±0.03	0.34	±0.03	0.33	±0.03	0.31	±0.03
H	0.21	±0.02	0.19	±0.02	0.17	±0.02	0.17	±0.02	0.18	±0.02
I	0.22	±0.03	0.35	±0.03	0.48	±0.03	0.60	±0.02	0.71	±0.03
J	0.90	±0.04	0.94	±0.03	0.98	±0.03	1.02	±0.03	1.04	±0.03
K	0.98	±0.04	0.83	±0.04	0.67	±0.04	0.51	±0.04	0.37	±0.04

Pluto Size Survey

	Rp = 1110 km		Rp = 1140 km		Rp = 1170 km		Rp = 1200 km		Rp = 1230 km	
A	0.62	±0.04	0.58	±0.04	0.54	±0.04	0.51	±0.04	0.49	±0.04
B	0.38	±0.04	0.35	±0.04	0.32	±0.04	0.27	±0.04	0.22	±0.04
C	0.60	±0.02	0.55	±0.02	0.51	±0.02	0.47	±0.02	0.44	±0.02
D	0.51	±0.02	0.56	±0.02	0.60	±0.02	0.63	±0.02	0.65	±0.02
E	0.55	±0.02	0.60	±0.02	0.66	±0.02	0.72	±0.02	0.78	±0.02
F	0.56	±0.03	0.51	±0.03	0.45	±0.03	0.40	±0.03	0.34	±0.03
G	0.37	±0.03	0.35	±0.03	0.31	±0.03	0.27	±0.03	0.23	±0.03
H	0.15	±0.02	0.17	±0.02	0.21	±0.02	0.26	±0.02	0.31	±0.02
I	0.46	±0.03	0.45	±0.03	0.44	±0.03	0.43	±0.03	0.42	±0.03
J	0.99	±0.03	0.97	±0.03	0.94	±0.03	0.92	±0.03	0.88	±0.03
K	0.74	±0.04	0.71	±0.04	0.69	±0.04	0.66	±0.04	0.65	±0.04

Semimajor Axis Survey

	A = 18750 km		A = 19000 km		A = 19250 km		A = 19500 km		A = 19750 km		A = 20000 km	
A	0.57	±0.03	0.56	±0.03	0.56	±0.03	0.57	±0.04	0.58	±0.04	0.59	±0.04
B	0.29	±0.04	0.32	±0.04	0.33	±0.04	0.34	±0.04	0.36	±0.04	0.40	±0.04
C	0.48	±0.02	0.50	±0.02	0.52	±0.02	0.54	±0.02	0.56	±0.02	0.57	±0.02
D	0.57	±0.02	0.58	±0.02	0.58	±0.02	0.57	±0.02	0.56	±0.02	0.56	±0.02
E	0.63	±0.02	0.62	±0.02	0.62	±0.02	0.61	±0.02	0.60	±0.02	0.58	±0.02
F	0.34	±0.02	0.39	±0.02	0.43	±0.02	0.48	±0.02	0.52	±0.03	0.57	±0.03
G	0.26	±0.02	0.29	±0.02	0.31	±0.02	0.33	±0.03	0.35	±0.03	0.38	±0.03
H	0.23	±0.02	0.20	±0.02	0.19	±0.02	0.18	±0.02	0.17	±0.02	0.16	±0.02
I	0.67	±0.02	0.60	±0.02	0.54	±0.02	0.48	±0.03	0.42	±0.03	0.36	±0.03
J	1.02	±0.03	1.01	±0.03	0.99	±0.03	0.97	±0.03	0.96	±0.03	0.95	±0.03
K	0.35	±0.04	0.46	±0.04	0.56	±0.04	0.66	±0.04	0.75	±0.04	0.84	±0.04

Tables 3.2 - 3.4 The panel albedos ± one standard deviation for the eleven panels (**A** through **K**) as a function of (a) Charon's radius, (b) Pluto's radius, and (c) Charon's semimajor axis.

It is difficult to make general statements about how shrinking or increasing one parameter relative to the other two will affect the surface map. One has to observe the change in coverage over Pluto's disk as the events progress. The effects depend largely on the specific panel locations as well as the geometry of the particular event. Typical panel sensitivities are as follows: a 10% change in the radius of Charon or the radius of Pluto typically corresponds to a 20% change in a panel's albedo, while a 6.5% change in the semimajor axis corresponds to an average change of approximately 25%. We notice that the panels with small areas (**A**, **B**, **J**, and **K** - the poles) or sparse coverage (panel **I**) are forced to take up most of the change when a scale length in the model is changed, whereas the panels with better coverage (C through **H**) remain relatively constant.

As an aside, we wonder whether the three surveys (tables 3.2 - 3.4) can be used to choose preferred values of Pluto's and Charon's radii and Charon's semimajor axis. In Figures 3.3 - 3.5 are the χ^2 values resulting from each of the fifteen fits. While these fifteen fits do not span the entire three dimensional parameter space defined by Pluto's and Charon's radii and Charon's semimajor axis, they function as a 'poor man's least squares fit' by showing us three slices through the parameter space.

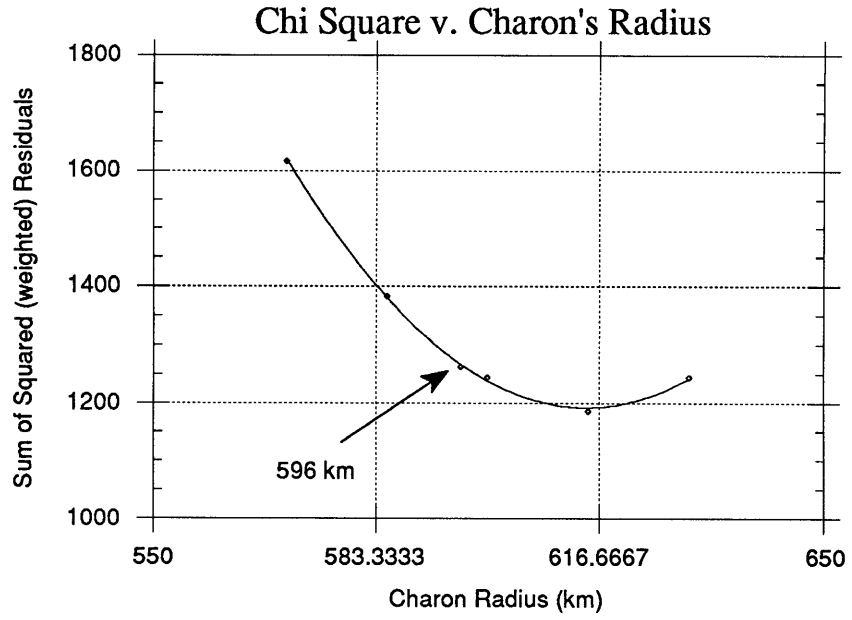

Figure 3.3 χ^2 as a function of Charon's radius. A second order polynomial fit through these six points has a minimum at approximately Rc = 615 km. In this fit Pluto's radius is 1142 km and Charon's semimajor axis is 19640 km.

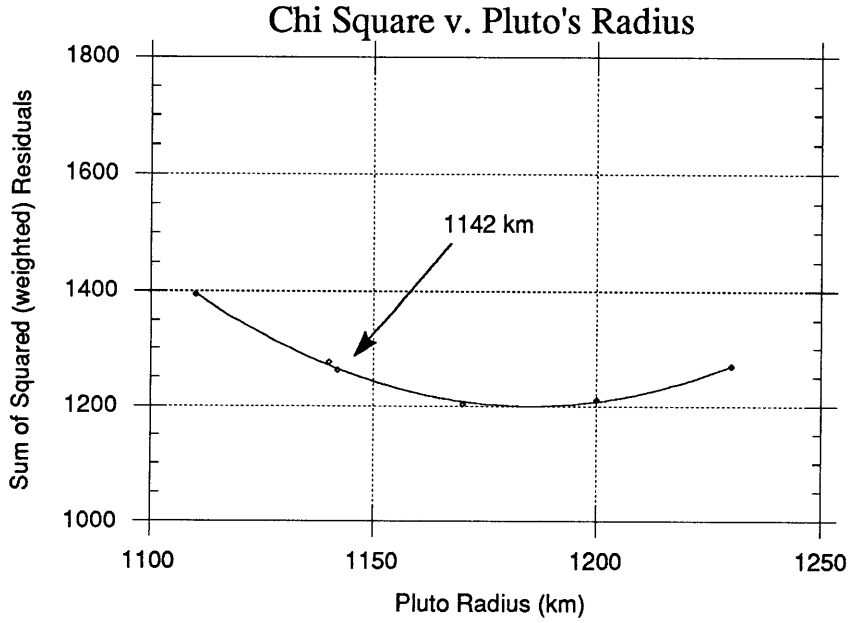

Figure 3.4 χ^2 as a function of Pluto's radius. A second order polynomial fit through these six points has a minimum at approximately Rp = 1183 km. In this fit Charon has a radius of 596 km and a semimajor axis of 19640 km.

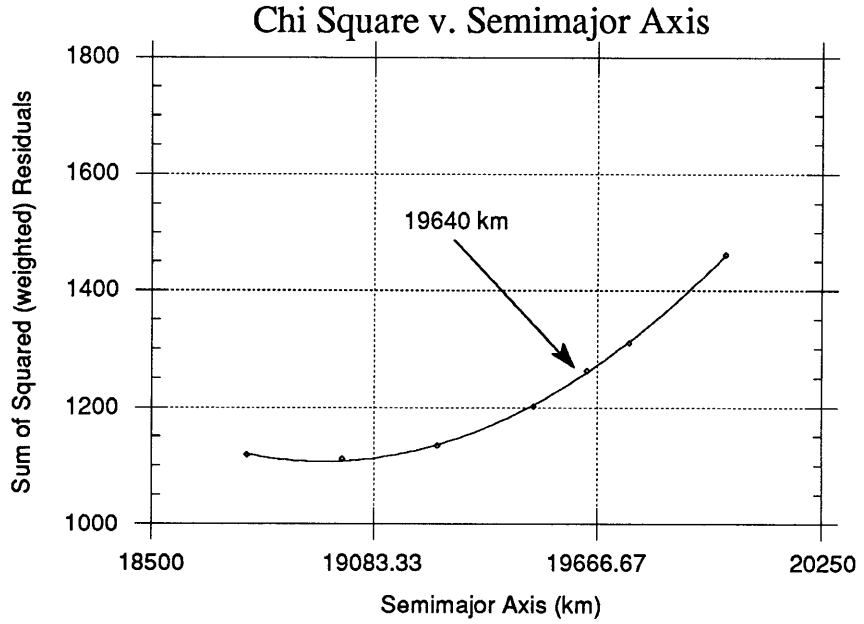

Figure 3.5 χ^2 as a function of Charon's semimajor axis. A second order polynomial fit through these seven points has a minimum at approximately A = 18945 km. In this fit Pluto's radius is 1142 km and Charon's radius is 596 km.

One might argue that the minimum χ^2 values *have* to match Buie and Tholen's values, since those values were derived from mutual event lightcurves in the first place. Our five lightcurves were not used in their calculation, however, and constitute independent corroboration (or contradiction) of their findings. We notice that Pluto's and Charon's radii, as indicated from the minimum χ^2 values, are 3.4% larger than Tholen's and Buie's recommended values, and the minimum χ^2 value for the semimajor axis is 3.3% smaller. Since Tholen and Buie have been refining the parameters of the Pluto-Charon system since 1986, we would be premature to abandon them in favor of the quick and dirty results of the minimum χ^2 parameters from Figures 3.3 - 3.5. Nevertheless, future studies should include a nonlinear fit of Charon's orbital parameters as well as the panel albedos.

Evaluating the Quality of the Fit

How well is the surface model able to predict the observed lightcurves? Below are the five observed lightcurves overlaid with the model predictions.

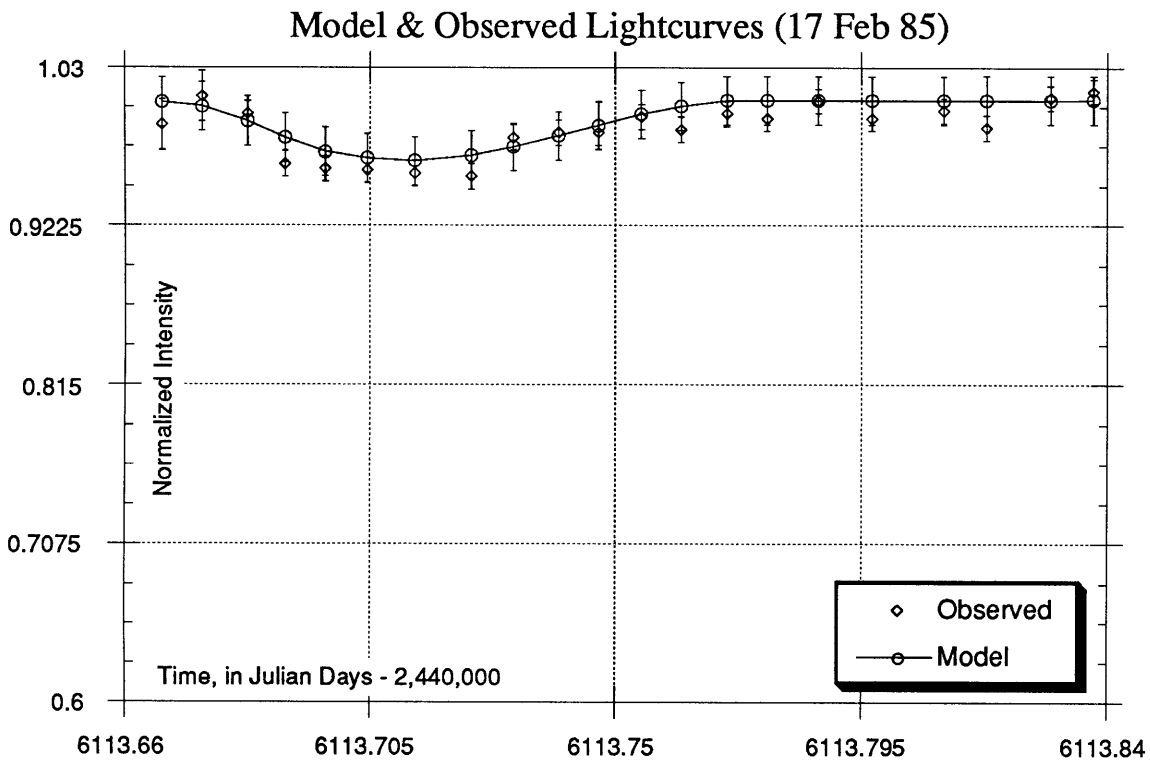
Model & Observed Lightcurves (17 Feb 85)
1.03
0.9225
0.815
0.7075
0.6
Normalized Intensity
Time, in Julian Days - 2,440,000
6113.66
6113.705
6113.75
6113.795
6113.84
Observed
Model

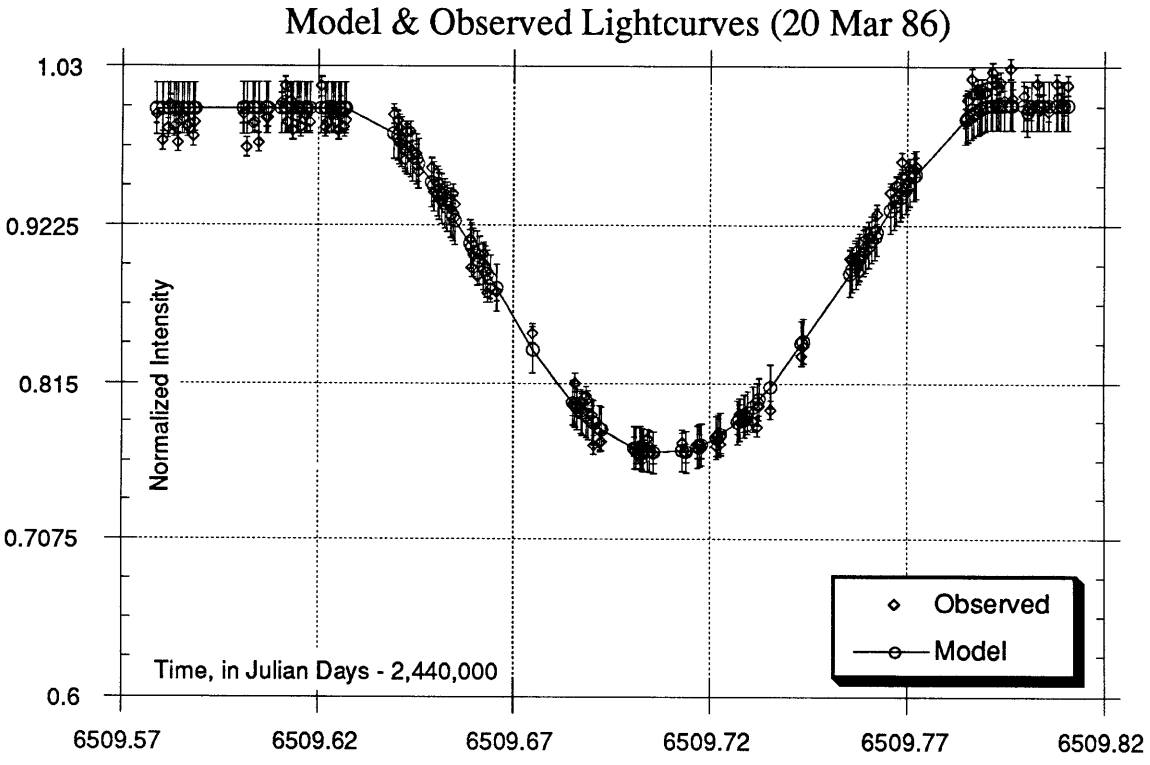
Model & Observed Lightcurves (20 Mar 86)
1.03
0.9225
0.815
0.7075
0.6
Normalized Intensity
Time, in Julian Days - 2,440,000
6509.57
6509.62
6509.67
6509.72
6509.77
6509.82
Observed
Model

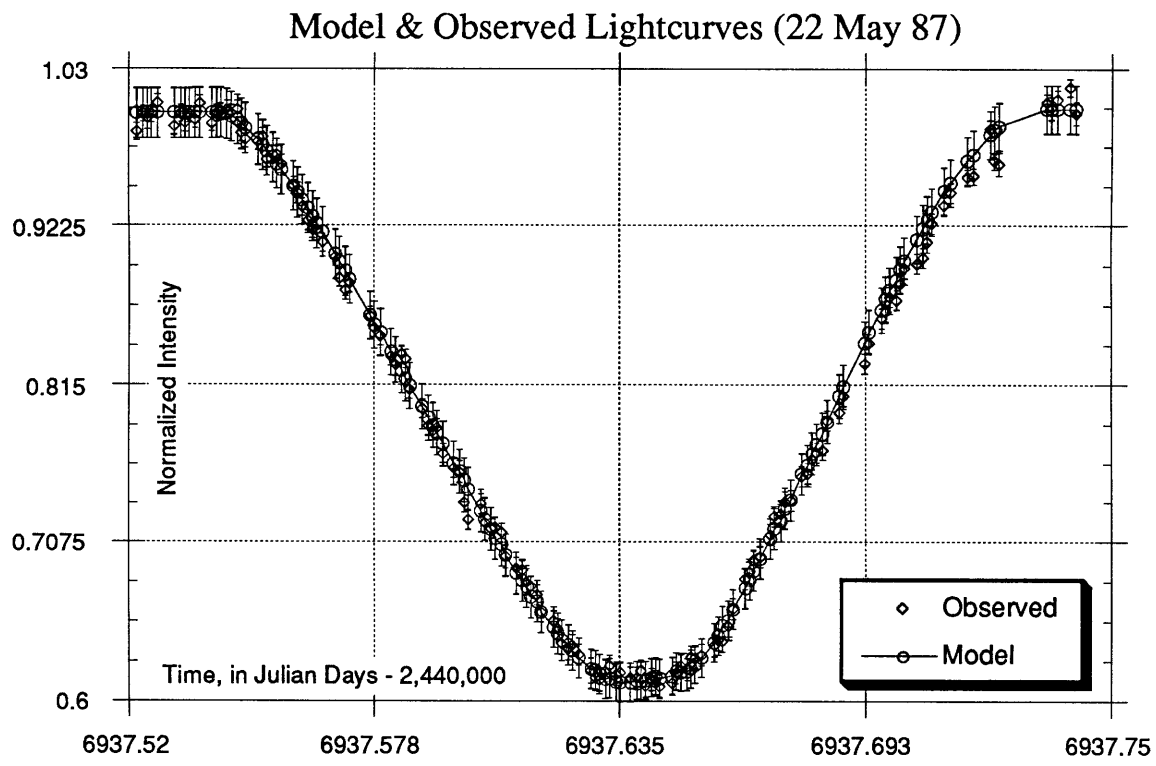
Model & Observed Lightcurves (22 May 87)
1.03
0.9225
0.815
0.7075
0.6
Normalized Intensity
Time, in Julian Days - 2,440,000
6937.52
6937.578
6937.635
6937.693
6937.75
Observed
Model

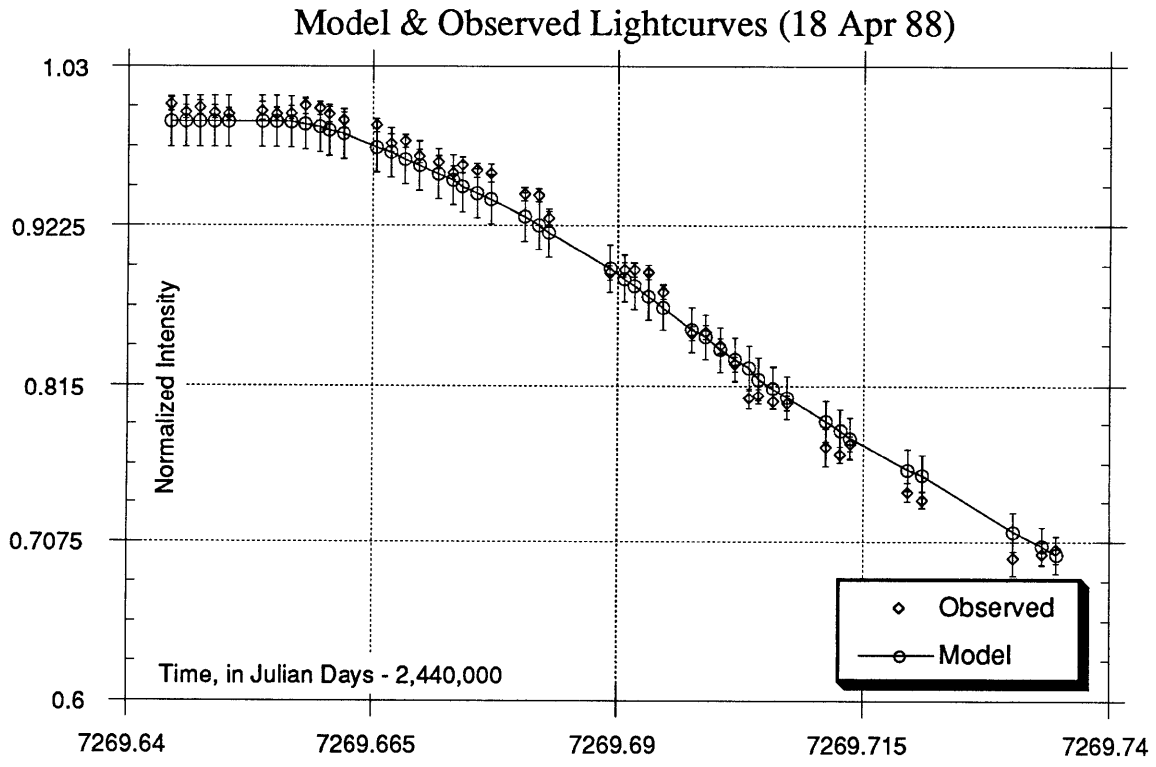
Model & Observed Lightcurves (18 Apr 88)
1.03
0.9225
0.815
0.7075
0.6
Normalized Intensity
Time, in Julian Days - 2,440,000
7269.64
7269.665
7269.69
7269.715
7269.74
Observed
Model

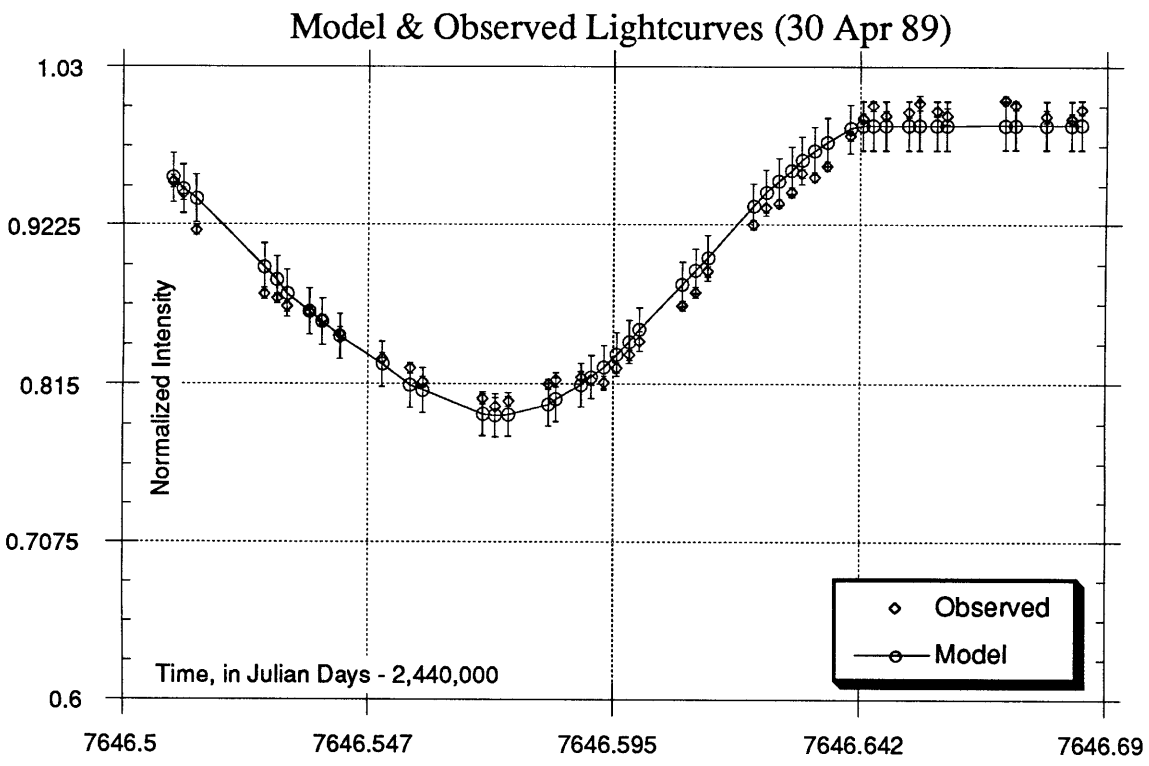

Figures 3.6 - 3.10

Lightcurves from 17 Feb. 85, 20 Mar. 86, 22 May 87, 18 Apr. 88, and 30 Apr. 89 respectively. Each graph shows the observed lightcurve overlaid with the model's predicted lightcurve. The X-axis is time, in Julian days (minus the 2,440,000). Error bars on the observed values represent either the Poisson noise or the local scatter (a standard deviation calculated from a two minute sample). The model lightcurve error bars are propagated from the formal least square errors of each panel albedo.

Figures 3.6 - 3.10 show that the surface map does a reasonably good job of recreating the observed lightcurves. An important issue is whether the surface map is a unique solution to the least squares problem. The traditional way to answer this question is to examine the off-diagonal elements of the normalized covariance matrix. The off-diagonal elements of the normalized covariance matrix should be 0 if two parameters are independent, 1 if there are exactly correlated, and -1 if they are anticorrelated. Off-diagonal elements that are too close to 1 indicate a two parameters that are not well distinguished by the data.

	A	B	C	D	E	F	G	H	I	J	K
1	1	-0.7258	-0.3657	-0.6294	0.30879	0.36466	0.07355	0.19795	-0.1523	-0.2312	0.1881
2	-0.7258	1	0.12781	0.50987	-0.64	-0.4007	0.03261	-0.2317	0.07701	0.28407	-0.0662
3	-0.3657	0.12781	1	-0.2448	0.22829	-0.1835	-0.5384	0.08852	-0.033	0.0447	0.04968
4	-0.6294	0.50987	-0.2448	1	-0.6092	0.06499	0.33449	-0.5345	0.08687	0.38325	-0.1354
5	0.30879	-0.64	0.22829	-0.6092	1	-0.1035	-0.2163	0.35229	-0.1988	-0.3534	0.19585
6	0.36466	-0.4007	-0.1835	0.06499	-0.1035	1	0.31637	-0.1458	-0.5321	0.03112	0.38072
7	0.07355	0.03261	-0.5384	0.33449	-0.2163	0.31637	1	-0.5668	-0.0841	-0.0045	0.17254
8	0.19795	-0.2317	0.08852	-0.5345	0.35229	-0.1458	-0.5668	1	-0.2971	-0.6663	0.22938
9	-0.1523	0.07701	-0.033	0.08687	-0.1988	-0.5321	-0.0841	-0.2971	1	0.32661	-0.8881
10	-0.2312	0.28407	0.0447	0.38325	-0.3534	0.03112	-0.0045	-0.6663	0.32661	1	-0.5163
11	0.1881	-0.0662	0.04968	-0.1354	0.19585	0.38072	0.17254	0.22938	-0.8881	-0.5163	1

Table 3.5. The normalized covariance matrix. The row numbers **1** through **11** refer to panels **A** through **K**.

We see that parameters 9 and 11 have a correlation coefficient of -0.89. Not surprisingly, these two parameters are the albedos of panels **I** and **K**, which occupy the part of Pluto least well covered by the data set, the southeast (bottom left) region. Is there insufficient data to warrant separating this region into two panels? We check the list of singular values.

	Singular Values
A	1081.29
B	159.322
C	155.555
D	74.1374
E	58.2718
F	45.0409
G	35.4388
H	32.2161
I	14.6245
J	18.7838
K	23.3375

Table 3.6. The singular values of the eleven parameters.

As described in Appendix B, the condition number (the ratio of the largest singular value to the smallest one) indicates whether any parameters are linear combinations of other parameters. In this case the largest singular value is 1081.29, the smallest is 14.6245. The condition number, 74.0, does not indicate any danger of degeneracy in the parameter space[8]. The solution is unique, but the covariance matrix points out that the data coverage in the south-

8. When is a condition number too large? In the singular value decomposition implementation of the least squares problem, the solutions can be written as

$$[\text{panel albedos}] = \sum_{i=1}^{M} \left(\frac{[U]_i \cdot \bar{b}}{w_i} \right) [V]_i$$

Equation 3.2, from page 535 of [Press et al 1988]

where M is the number of parameters in the fit and the w's are the singular values. As pointed out in Numerical Recipes in

east quadrant is thin.

The Limb Darkening Parameter

The Minnaert law empirically describes limb darkening of planetary objects. In Pluto's case, we have:

$$I(\theta) = I_0 \cos^{2k-1}\theta$$

Equation 3.3. The Minnaert limb darkening law. θ is the angle from the center of the planet's disk to a point on the disk measured from the center of the planet. θ ranges from 0° to 90°.

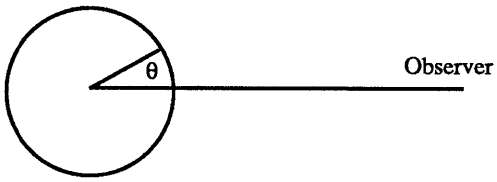

Figure 3.11. Definition of θ.

We solved for a value of k, the Minnaert exponent, by trying a range of values from k = 0 to k = 1.5, and plotted the resulting χ^2 values as a function of k. The Minnaert parameter which yielded the minimum χ^2 value is k = 0.53. A value of k = 0.5 corresponds to the case in which there is no limb effect. Values of k smaller than 0.5 correspond to limb brightened planets (such as Uranus in the 2 micron band) whereas values greater than 0.5 correspond to limb darkened planets, which includes most bright, scattering planets.

section 14.3, the solutions are linear combinations of the columns of [V], with the i^{th} singular value appearing in a crucial position in the denominator of the coefficient of $[V]_i$. If a particular w_i is very large compared to the smallest singular value, then the i^{th} column of [V] will not be well represented in the linear combination. Numerical Recipes recommends a condition number less than $1/(N\,\varepsilon)$, where N is the number of data points and ε is the machine precision. Our condition number is much smaller than this recommended limit.

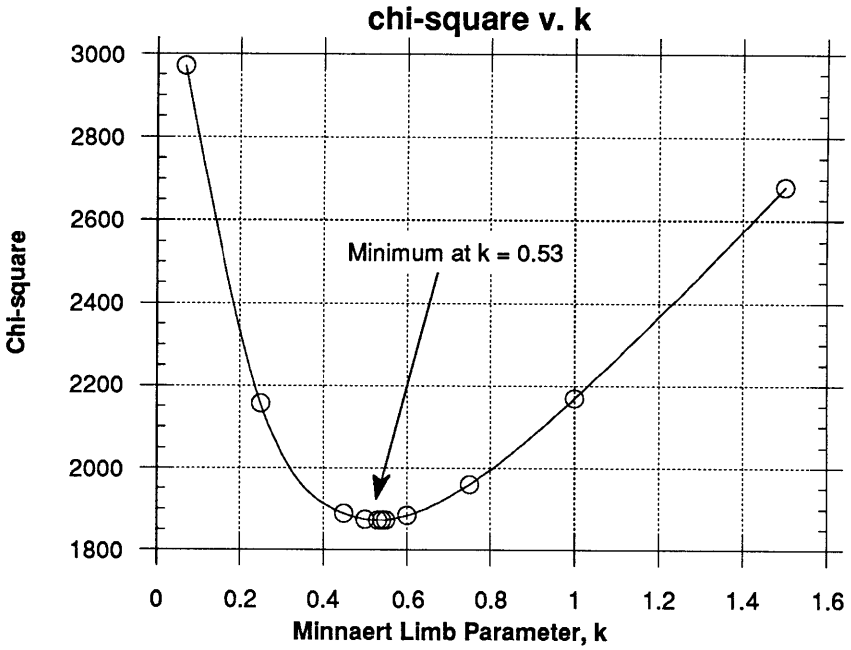

Figure 3.12. χ^2 as a function of the Minnaert limb darkening parameter. A value of k = 0.5 indicates no limb darkening effect. The value of 0.53 indicates some limb darkening, but less than is generally expected for an object as bright as Pluto.

We have recalculated the eleven panel map albedos with the Minnaert law incorporated into our model for k = 0.53 as well as k = 0.5. The case in which k = 0.5 is identical to the case shown earlier (Figure 3.2), but is shown here as a check on the new model.

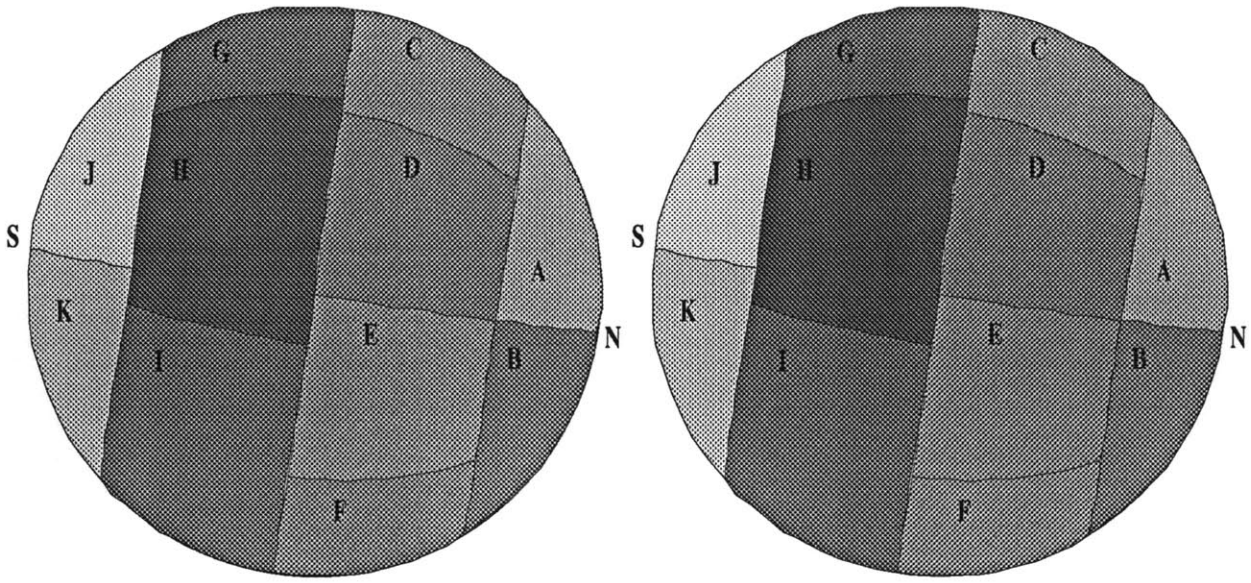

Geometric Albedos

	k = 0.5	k = 0.53
A	0.69 ±0.041	0.70 ±0.042
B	0.43 ±0.045	0.45 ±0.046
C	0.57 ±0.023	0.59 ±0.023
D	0.50 ±0.022	0.49 ±0.022
E	0.58 ±0.022	0.55 ±0.021
F	0.53 ±0.028	0.55 ±0.028
G	0.33 ±0.030	0.34 ±0.031
H	0.25 ±0.023	0.23 ±0.022
I	0.37 ±0.027	0.37 ±0.027
J	0.87 ±0.034	0.90 ±0.035
K	0.81 ±0.043	0.84 ±0.045

Figure 3.13. A comparison of the eleven panel maps for k = 0.5 (left side, no limb effects) and k = 0.53 (right side, slightly limb darkened).

Below are the covariance and normalized covariance matrices for k = 0.53.

	A	B	C	D	E	F	G	H	I	J	K
1	0.00181	-0.0015	-0.0004	-0.0006	0.00029	0.00045	0.0001	0.00019	-0.0002	-0.0004	0.00035
2	-0.0015	0.00224	0.00015	0.00054	-0.0006	-0.0006	4.1E-05	-0.0002	0.0001	0.00048	-0.0001
3	-0.0004	0.00015	0.00055	-0.0001	0.00012	-0.0001	-0.0004	4.8E-05	-2E-05	3.8E-05	5E-05
4	-0.0006	0.00054	-0.0001	0.00049	-0.0003	4.4E-05	0.00023	-0.0003	5.1E-05	0.00031	-0.0001
5	0.00029	-0.0006	0.00012	-0.0003	0.00047	-6E-05	-0.0001	0.00017	-0.0001	-0.0003	0.0002
6	0.00045	-0.0006	-0.0001	4.4E-05	-6E-05	0.00084	0.00029	-1E-04	-0.0004	3.3E-05	0.0005
7	0.0001	4.1E-05	-0.0004	0.00023	-0.0001	0.00029	0.00098	-0.0004	-7E-05	-6E-06	0.00024
8	0.00019	-0.0002	4.8E-05	-0.0003	0.00017	-1E-04	-0.0004	0.00052	-0.0002	-0.0005	0.00024
9	-0.0002	0.0001	-2E-05	5.1E-05	-0.0001	-0.0004	-7E-05	-0.0002	0.00076	0.00033	-0.0011
10	-0.0004	0.00048	3.8E-05	0.00031	-0.0003	3.3E-05	-6E-06	-0.0005	0.00033	0.00131	-0.0009
11	0.00035	-0.0001	5E-05	-0.0001	0.0002	0.0005	0.00024	0.00024	-0.0011	-0.0009	0.00206

Table 3.7. The covariance matrix from the eleven panel least squares fit with k = 0.53. The row numbers **1** through **11** refer to panels **A** through **K**.

	A	B	C	D	E	F	G	H	I	J	K
1	1	-0.736	-0.3687	-0.6263	0.31098	0.36678	0.07594	0.19517	-0.145	-0.2296	0.18148
2	-0.736	1	0.13165	0.51137	-0.6358	-0.4046	0.02766	-0.2272	0.07867	0.28145	-0.0669
3	-0.3687	0.13165	1	-0.2476	0.2301	-0.1897	-0.545	0.0901	-0.0288	0.04449	0.04707
4	-0.6263	0.51137	-0.2476	1	-0.6109	0.06745	0.33631	-0.5321	0.08266	0.38125	-0.1324
5	0.31098	-0.6358	0.2301	-0.6109	1	-0.1032	-0.2174	0.35224	-0.2044	-0.3546	0.20081
6	0.36678	-0.4046	-0.1897	0.06745	-0.1032	1	0.31891	-0.1464	-0.5288	0.03189	0.37661
7	0.07594	0.02766	-0.545	0.33631	-0.2174	0.31891	1	-0.5664	-0.0776	-0.0054	0.1663
8	0.19517	-0.2272	0.0901	-0.5321	0.35224	-0.1464	-0.5664	1	-0.3039	-0.6665	0.23608
9	-0.145	0.07867	-0.0288	0.08266	-0.2044	-0.5288	-0.0776	-0.3039	1	0.33316	-0.8884
10	-0.2296	0.28145	0.04449	0.38125	-0.3546	0.03189	-0.0054	-0.6665	0.33316	1	-0.5229
11	0.18148	-0.0669	0.04707	-0.1324	0.20081	0.37661	0.1663	0.23608	-0.8884	-0.5229	1

Table 3.8. The normalized covariance matrix from the eleven panel least squares fit with k = 0.53. The row numbers **1** through **11** refer to panels **A** through **K**.

Comparison to Earlier Surface Maps

The two models discussed in Chapter Two differ from the eleven panel map in two important regards: (a) they were constructed before mutual event data could be incorporated, and (b) they model the entire surface of Pluto, not just the Charon-facing hemisphere. The SHELF model [Buie, M.W. and Tholen, D.J. 1988] supersedes the earlier two-spot model [Marcialis, R.L. 1983], and is the main subject of this comparison.

The SHELF model has 22 fitted parameters, compared to 11 for the eleven panel map, but since the eleven panel map only covers the sub-Charon hemisphere of Pluto, the number of free parameters per hemisphere is the same. Indeed, because the SHELF model's equatorial spots are located on the anti-Charon side of Pluto, the SHELF model's sub-Charon side is remarkably similar to the eleven panel map.

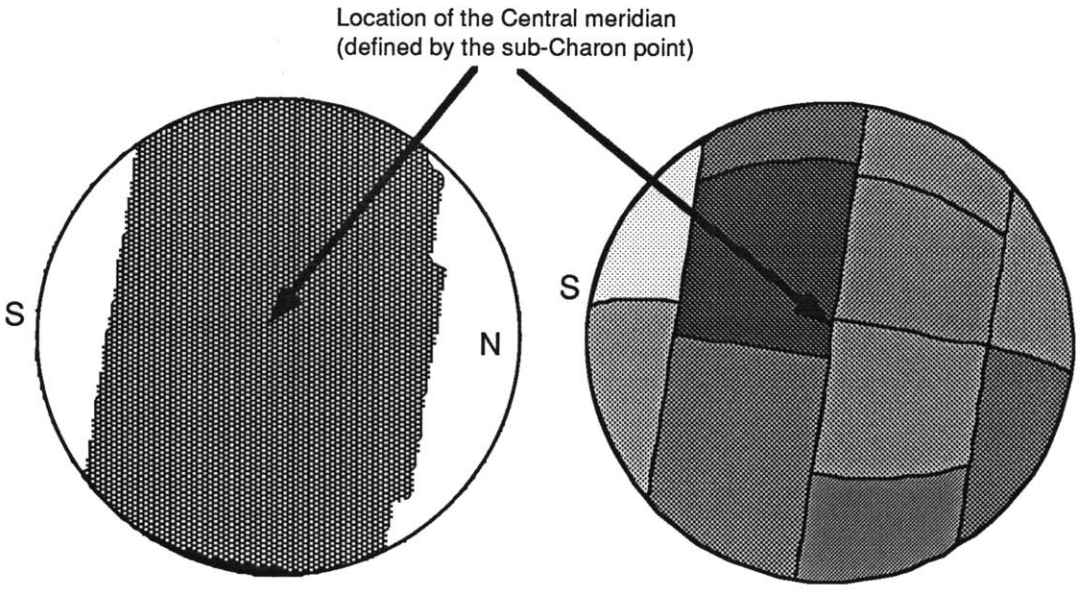

Figure 3.14 A comparison of the SHELF model (left) and the eleven panel model (right). Notice that the SHELF model's two equatorial spots are both hidden from view when Pluto's sub-

Charon point faces the Earth. We can barely see the edge of the SHELF model's dark spot, and it disappears completely soon after the event begins.

The important differences are (a) the SHELF model incorporates an average particle phase function, which the eleven panel map attempts to represent with Minnaert limb darkening, and (b) the eleven panel map shows a roughly uniform northern hemisphere, while the SHELF model shows a north pole cap that is strikingly different from the rest of the northern hemisphere. Figure 3.14 compares the eleven panel model surface map with the corresponding view of the SHELF model, and Figure 3.15 (below) shows how the delineations of the two maps compare.

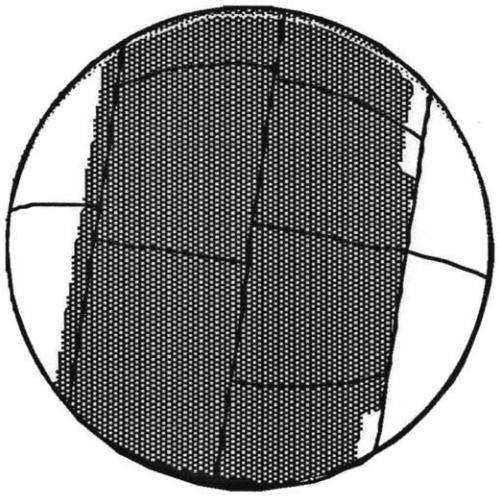

Figure 3.15 The SHELF model overlaid by the eleven panel map. We expect mutual events which cover the northern hemisphere to distinguish between the two models.

To test the relative accuracy of the SHELF model we generated lightcurves from the model and compared them to the observed lightcurves. The 1986 and 1987 events cover the northern hemisphere, so these are the critical events to look at. In the 1986 event, the SHELF model's cap region is covered by Charon. If the cap is too bright in the SHELF model, we expect the synthetic lightcurve to fall below the observed lightcurve as the unrealistically bright polar cap is covered up. In the 1987 event more of the northern equatorial region is covered in midevent. If the SHELF model representation of this region is too dim, then the SHELF lightcurve will not be as deep as the observed lightcurve. The SHELF lightcurve is both too shallow in 1987 and too deep in 1986. We believe that the *a priori* assumption of a "spot" over the north pole, combined with the fact the SHELF model was not based on any mutual event lightcurves, has led to a differentiated northern hemisphere on Pluto. Despite the fact that the SHELF model was constructed solely from rotational lightcurves, its fit to the observed lightcurves is very good for the 1988 - 1990 events.

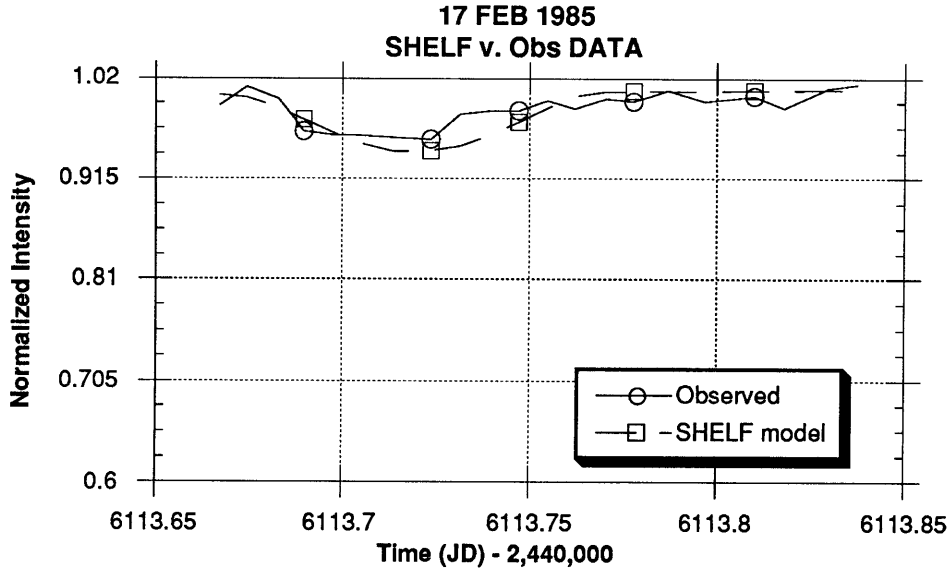
17 FEB 1985
SHELF v. Obs DATA
1.02
0.915
0.81
0.705
0.6
Normalized Intensity
6113.65
6113.7
6113.75
6113.8
6113.85
Time (JD) - 2,440,000
Observed
SHELF model

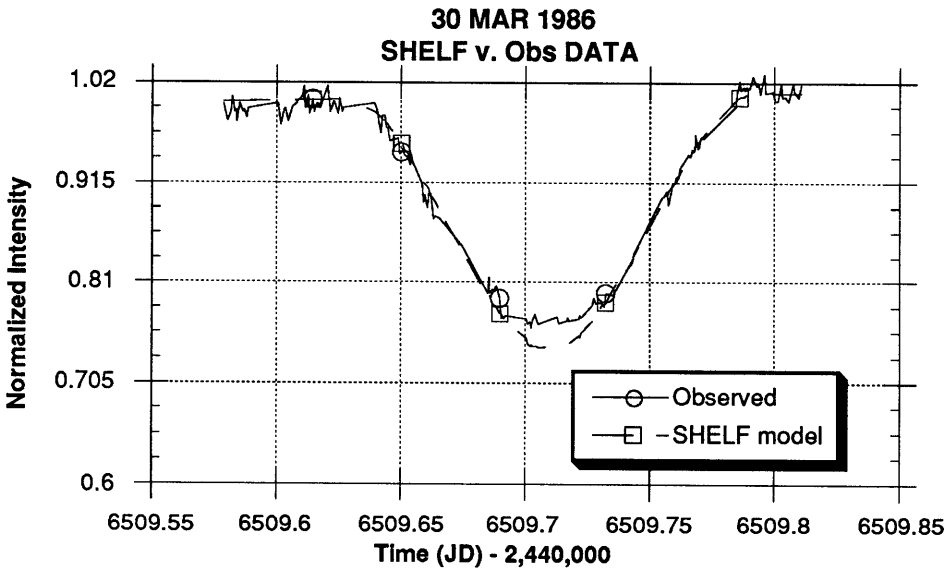
30 MAR 1986
SHELF v. Obs DATA
1.02
0.915
0.81
0.705
0.6
Normalized Intensity
6509.55
6509.6
6509.65
6509.7
6509.75
6509.8
6509.85
Time (JD) - 2,440,000
Observed
SHELF model

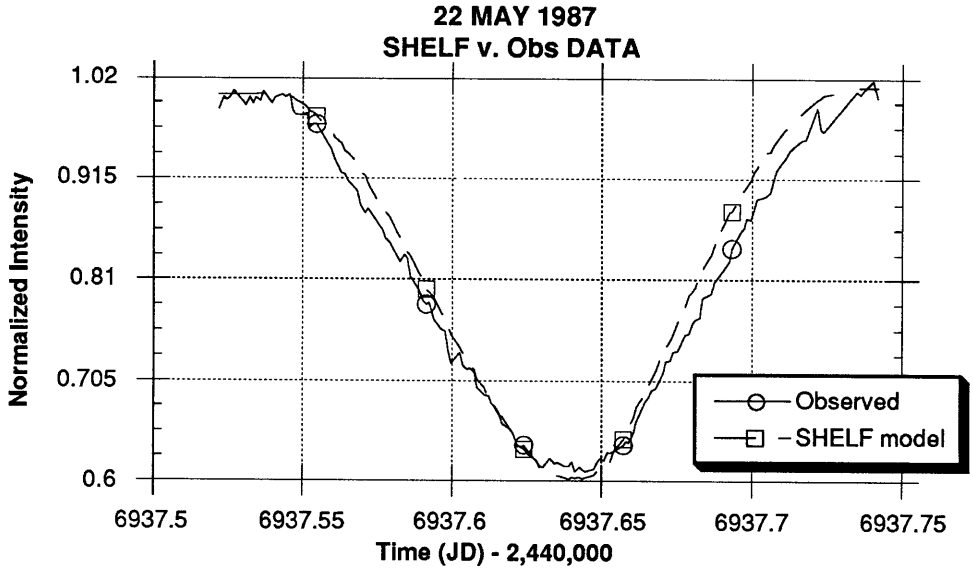
22 MAY 1987
SHELF v. Obs DATA
1.02
0.915
0.81
0.705
0.6
Normalized Intensity
6937.5
6937.55
6937.6
6937.65
6937.7
6937.75
Time (JD) - 2,440,000
Observed
SHELF model

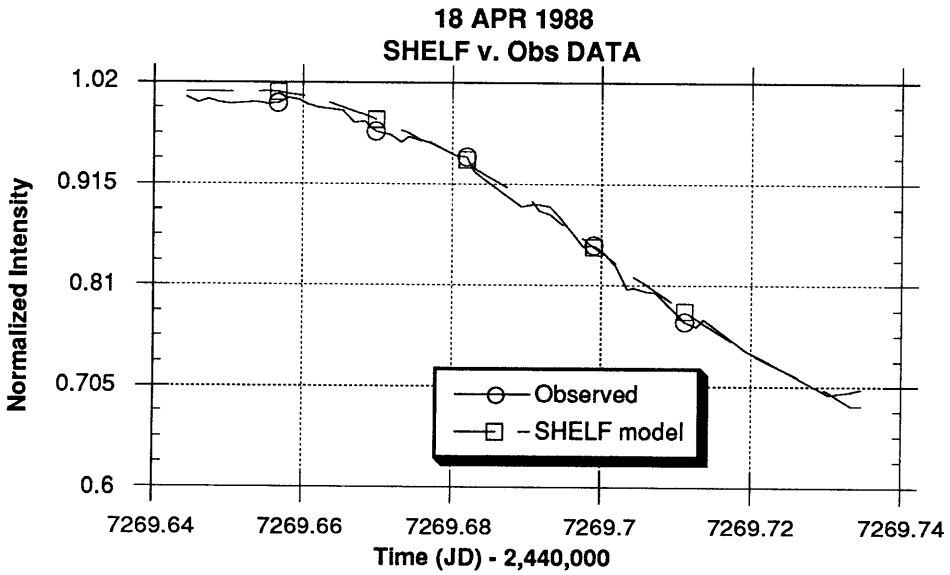
18 APR 1988
SHELF v. Obs DATA
1.02
0.915
0.81
0.705
0.6
Normalized Intensity
7269.64
7269.66
7269.68
7269.7
7269.72
7269.74
Time (JD) - 2,440,000
Observed
SHELF model

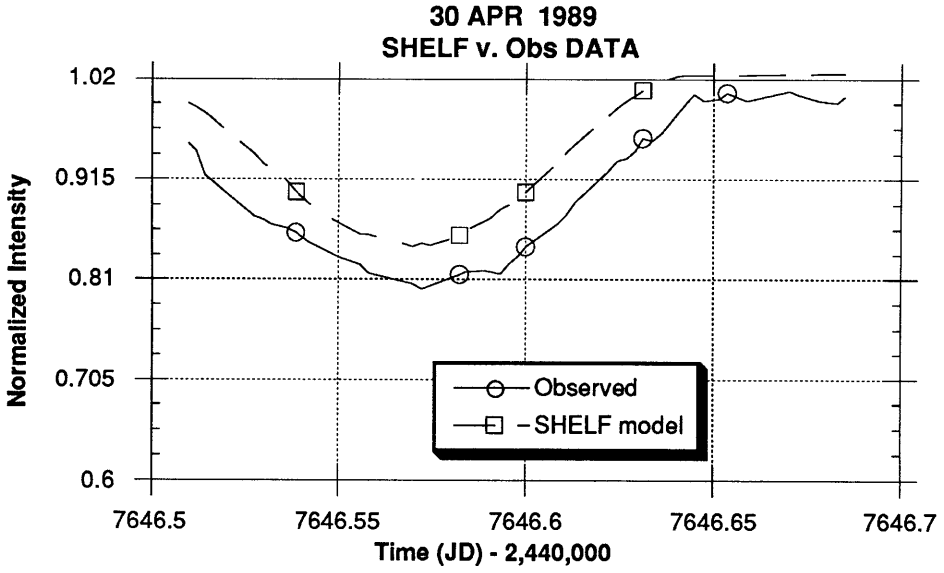

Figures 3.15 - 3.20 SHELF v. observed lightcurves for mutual events occurring in 1985 through 1989.

We believe that the 1986 event shows the north pole of Pluto to be less bright than the SHELF model predicts. The SHELF model predicts a deeper event minimum than is actually observed, indicating that the north polar cap of the SHELF model is too bright.

The 1989 comparison (Figure 3.20, above) points out a problem we had in scaling the SHELF model's synthetic lightcurves. The output of the SHELF model is a bidirectional reflectance at every point on Pluto's disk, as opposed to relative brightnesses which add up to the total geometric albedo in the case of the eleven panel map. The conversion from geometric albedo to normal reflectance should be straightforward[9]. Nevertheless, we had difficulty in finding a consistent scale factor between the SHELF lightcurves and the normalized observed lightcurves.

9. In chapter 9 the book **Planetary Satellites** (Arizona Press), J. Ververka discusses the relation between normal reflectance, r_n, and geometric albedo, p. He points out that for an object with no limb darkening, $p = r_n$. For a Lambert sphere, $p = (2/3)\, r_n$. In general, the relation is

$$(k + 0.5)\, p = r_n$$

where k is the Minnaert parameter.

Now, we have a value for k or 0.53, but the output of the SHELF model indicates an average normal reflectance of approximately 0.2, relative to the geometric albedo of about 0.5, indicating a value for k close to zero. In other words, the output from the SHELF model does not compare to the geometric albedo the way we expected it to.

Chapter Four

Discussion of Results and Recommendations for Further Study

Pluto taken as a whole is an unusually bright planetary object. The accepted explanation for Pluto's overall brightness is that methane condenses often enough to provide a fresh layer of bright frost [S. A. Stern et al 1988]. The major differences in surface brightness on Pluto's disk can be attributed to either uneven frost depositions (e.g., preferential recondensation at the poles), or uneven frost sublimation, leaving more dark material mixed in with the frost. Since the poles intercept a smaller flux due to their oblique orientation to the Sun, we would expect solid methane to preferentially recondense at the poles and sublimate from the equator. Although the map shows strong evidence for a frost cap on the south pole, the presence of such a cap on the north pole is less obvious.

Recent pictures from Voyager [Smith, B.A., et al. 1989] show that Triton has a polar cap that seems to be receding on the sunward hemisphere [Veverka, J. 1989]. The explanation is that frost sublimates from the more heated pole and condenses onto the colder one. Both Triton and Pluto have long seasons in which one pole is preferentially in sunlight and the other is in darkness. Yet on Pluto we observe the South pole to be much brighter than the North, even though the South pole has been closer to the sun for the last 120 years. One explanation for this behavior depends on Pluto's atmosphere. Given that the methane component of Pluto's atmosphere freezes out as Pluto approaches aphelion and reforms as Pluto approaches perihelion, and given that subsolar point is at Pluto's equator at perihelion (with the South pole pointing in the direction of Pluto's orbital travel), we expect that the South pole will be the major reservoir for solid methane. Unlike Triton, Pluto's atmosphere does not maintain a constant pressure throughout the Pluto year. The methane component of the atmosphere freezes out when Pluto is far from the Sun. Recondensation of methane occurs during *post perihelion quarter only*, during which time the South pole is anti-sunward, and thus accumulates most of the new frost. Since Pluto's axis has had this tangential orientation at perihelion for some time [Dobrovolskis, A.R. and Harris, A.W. 1983], then the major portion of Pluto's transient methane reservoir should be located at the South pole.

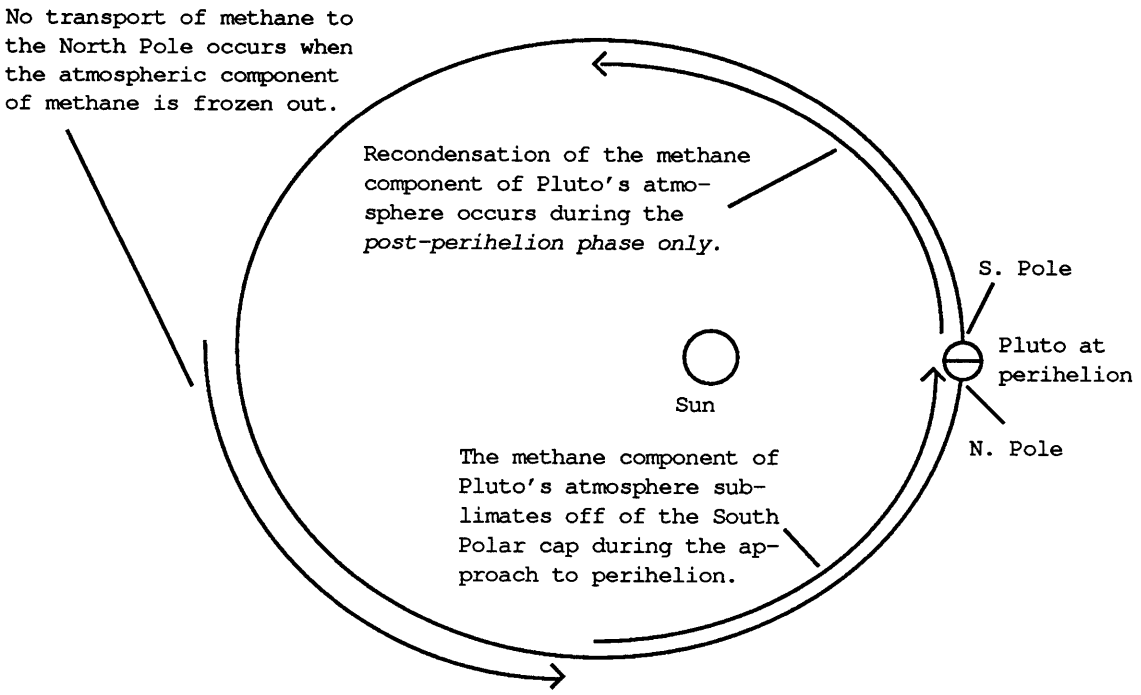

Figure 4.1. The preferential condensation of methane on Pluto.

We believe that Pluto's atmosphere is a factor in the large scale albedo features on Pluto. Modeling the interactions between Pluto's surface and its atmosphere should be a challenging and fruitful area of study.

Future Study

The Rest of the Data

Although the last mutual events are occurring this summer (August 1990), there is still a large body of data yet to be incorporated into the least squares panel map. The five year data set from McDonald observatory includes over 22 usable lightcurves. About half of the lightcurves are from inferior events (Charon in front), half are from superior. Incorporation of the additional lightcurves, along with a more systematic method for choosing the panel configuration, are the chief means by which we hope to achieve higher resolution on our next map. The additional inferior-event lightcurves should allow us to increase the map resolution by a factor of two. All of the features suggested by the sample map should be checked with a higher resolution map. What is the extent of the south polar cap? Is there a north polar cap, and what is its extent? There are bound to be large features on Pluto which the eleven panel map has averaged into even larger panels.

The Optimum Panel Map

Choosing the optimum panel map is an unsolved problem. If the panels contain regions of varying surface

brightnesses, then the panel brightnesses will average the variations. It would be better to have the panel borders coincide with the actual variations on the surface of the planet. The better choice of panels will result in smaller χ^2 values. We need a systematic way of choosing the panel configuration that leads to the smallest possible χ^2 value. Other researchers [Horne, K., Buie, M., and Tholen, D.J. 1988] are using a maximum entropy method to find the surface that yields the smallest χ^2 value.

Fitting Additional Parameters

The current model is linear, and solves for panel brightnesses in a single iteration. We should, however, be able to fit for a phase function as well as a single scattering albedo. Furthermore, we should incorporate a model of the atmosphere, which may be a significant factor, especially near the limb of the planet. A nonlinear least squares routine should be implemented to solve for these parameters.

The orbital parameters for Charon, Charon's radius, and Pluto's radius should also be incorporated as fitted parameters into the next nonlinear fit. Figures 3.3 - 3.5 indicate that our current values for Pluto's and Charon's radii may be too small, and Charon's semimajor axis value may be too large. The semimajor axis cannot be determined from the timing of the mutual events. We should determine an independent estimate of the semimajor axis from stellar occultation results.

Including Charon; Rotational Lightcurves

Finally, since we have lightcurves from superior as well as inferior events, we can construct a map of Charon in the same manner as we did for Pluto. In fact, a complete treatment of this problem would include rotational lightcurves and 360° maps of Pluto and Charon, with longitudinally resolved panels on the anti-Charon side of Pluto and the anti-Pluto side of Charon.

Appendix A

The Data Set

The detector used in these observations was an RCA 8850 phototube. Blue and visual Johnson filters were used on alternating integrations. Each integration was slightly less than 10 seconds. Sky counts were taken within five minutes of every data point. A comparison star was checked approximately once every half hour. The lightcurves used in this thesis were based exclusively on the blue Johnson filter integrations.

After correcting for extinction and subtracting the background, Charon's contribution to the lightcurve (assumed to be constant throughout the whole inferior event) was removed. The pre- and post-contact parts of the lightcurve were scaled to one, so all of the lightcurves could be concatenated into a single set.

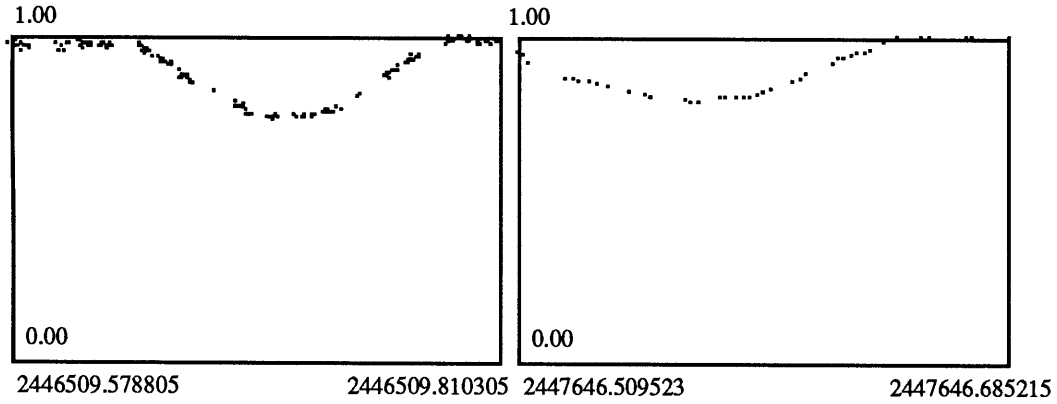

Figure C.1
The data set on the left was obtained in 1986, the right-hand data set was obtained in 1989. In both cases the intensities have been scaled so that the baseline value averages one. The abscissa is measured in Julian days.

To remove Charon's contribution from the observed intensity, we have to assume that Charon's anti-Pluto side is the same brightness as its Pluto-facing side. What is the effect of this assumption? Since the location of the minimum χ^2 depends on the derivative of the model (which is just the sum of the panel albedos plus a constant for Charon's contribution), removing a constant from each point in the photometric time series does not alter the relative brightnesses found by the least squares algorithm. The constant dissappears from the expression for the location of the χ^2 minimum in the least squares solution. The signal to noise ratio is affected, however, by removing the wrong constant value from the lightcurve.

We know that the Pluto-Charon magnitude decreases to 84.7% of the baseline value during a total superior event [Binzel, R. P. 1988]. We remove Charon's contribution to the intensity by subtracting 15.3 % of the average baseline value from every point.

There are six separate data sets used in this paper. The data sets are listed below. The abscissa is in Julian days, the ordinate is in normalized Pluto intensities. There are a total of 483 points in the six sets.

17 Feb 85

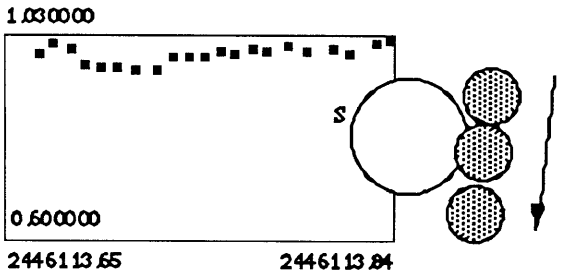

Julian Date	Normalized Intensity	± Sigma
2446113.666859	0.990946	0.017313
2446113.674276	1.010531	0.017313
2446113.682609	0.998523	0.008657
2446113.689526	0.964277	0.008657
2446113.696943	0.961118	0.008657
2446113.704359	0.960067	0.008657
2446113.713609	0.957967	0.008657
2446113.723776	0.955872	0.008657
2446113.731443	0.982345	0.008657
2446113.739526	0.985563	0.008657
2446113.747193	0.985563	0.008657
2446113.755026	0.996353	0.008657
2446113.762443	0.987713	0.008657
2446113.770568	0.998523	0.008657
2446113.777943	0.995270	0.008657
2446113.787234	1.007244	0.008657
2446113.796693	0.995270	0.008657
2446113.809901	1.000698	0.008657
2446113.817776	0.988789	0.008657
2446113.829818	1.009434	0.008657
2446113.837234	1.013827	0.008657

20 Mar 86

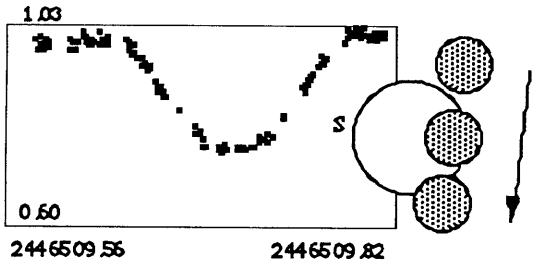

Julian Date	Normalized Intensity	± Sigma
2446509.578820	0.997959	0.006519
2446509.580111	0.979649	0.006519
2446509.581403	0.988230	0.006519
2446509.582070	1.004491	0.006519
2446509.582778	0.989307	0.006519
2446509.583486	0.990385	0.006519
2446509.584153	0.978581	0.006519
2446509.584861	0.997959	0.006519
2446509.585570	0.994707	0.006519
2446509.586236	0.989307	0.006519
2446509.586945	0.991464	0.006519
2446509.587653	0.982860	0.006519
2446509.588236	0.992544	0.006519
2446509.600820	0.997959	0.006519
2446509.601528	0.975382	0.006519
2446509.602903	0.991464	0.006519
2446509.603611	0.992544	0.006519
2446509.604320	0.978581	0.006519
2446509.606403	0.995790	0.006519
2446509.607070	0.995790	0.006519
2446509.610570	1.005583	0.006519
2446509.611236	1.016559	0.006519
2446509.611945	0.992544	0.006519
2446509.612653	1.006676	0.006519
2446509.613320	0.987154	0.006519
2446509.614028	0.995790	0.006519
2446509.614736	1.002309	0.006519
2446509.615403	0.989307	0.006519
2446509.616111	0.997959	0.006519
2446509.616820	0.996874	0.006519
2446509.617486	0.992544	0.006519
2446509.620736	1.016559	0.006519
2446509.621445	0.989307	0.006519
2446509.622111	0.992544	0.006519
2446509.622820	1.000132	0.006519
2446509.623528	0.997959	0.006519
2446509.624195	0.992544	0.006519
2446509.624903	0.987154	0.006519
2446509.625611	1.003400	0.006519
2446509.626278	0.989307	0.006519
2446509.626861	0.993625	0.006519
2446509.639278	0.997959	0.006519
2446509.639945	0.993625	0.006519
2446509.640653	0.988230	0.006519
2446509.641320	0.977514	0.006519
2446509.642028	0.966896	0.006519
2446509.642736	0.986079	0.006519
2446509.643403	0.986079	0.006519
2446509.644111	0.973255	0.006519
2446509.644820	0.971131	0.006519
2446509.645528	0.958472	0.006519
2446509.648736	0.961623	0.006519
2446509.649445	0.944914	0.006519
2446509.650153	0.946989	0.006519
2446509.650820	0.951151	0.006519
2446509.651528	0.943878	0.006519
2446509.652236	0.941808	0.006519
2446509.652903	0.942842	0.006519
2446509.653611	0.933568	0.006519
2446509.654320	0.943878	0.006519
2446509.654986	0.936651	0.006519
2446509.658486	0.913231	0.006519
2446509.659153	0.894256	0.006519
2446509.659861	0.902205	0.006519

2446509.660570	0.888332	0.006519
2446509.661236	0.903203	0.006519
2446509.661945	0.903203	0.006519
2446509.662653	0.891290	0.006519
2446509.663320	0.876582	0.006519
2446509.664028	0.879508	0.006519
2446509.665403	0.877556	0.006519
2446509.674695	0.848718	0.006519
2446509.684861	0.798774	0.006519
2446509.685570	0.815147	0.006519
2446509.686236	0.798774	0.006519
2446509.686945	0.802389	0.006519
2446509.687653	0.801484	0.006519
2446509.688320	0.806017	0.006519
2446509.689028	0.803295	0.006519
2446509.689736	0.792480	0.006519
2446509.690403	0.772082	0.006519
2446509.691820	0.773839	0.006519
2446509.692361	0.774719	0.006519
2446509.700611	0.771205	0.006519
2446509.701278	0.765960	0.006519
2446509.701986	0.768579	0.006519
2446509.702695	0.761611	0.006519
2446509.703361	0.769454	0.006519
2446509.704070	0.776480	0.006519
2446509.704778	0.771205	0.006519
2446509.705445	0.765960	0.006519
2446509.713111	0.773839	0.006519
2446509.713778	0.766832	0.006519
2446509.716570	0.769454	0.006519
2446509.717278	0.772960	0.006519
2446509.717945	0.769454	0.006519
2446509.721445	0.771205	0.006519
2446509.722111	0.775599	0.006519
2446509.722820	0.772960	0.006519
2446509.726861	0.786226	0.006519
2446509.727570	0.793377	0.006519
2446509.728278	0.788009	0.006519
2446509.728945	0.788009	0.006519
2446509.729653	0.788901	0.006519
2446509.731028	0.788009	0.006519
2446509.731736	0.784447	0.006519
2446509.732445	0.798774	0.006519
2446509.735320	0.796072	0.006519
2446509.743195	0.833660	0.006519
2446509.743778	0.840220	0.006519
2446509.755236	0.900212	0.006519
2446509.755945	0.900212	0.006519
2446509.756611	0.906202	0.006519
2446509.757320	0.898223	0.006519
2446509.758028	0.891290	0.006519
2446509.758695	0.905201	0.006519
2446509.759403	0.914239	0.006519
2446509.760070	0.915248	0.006519
2446509.760778	0.915248	0.006519
2446509.761486	0.920307	0.006519
2446509.762153	0.930494	0.006519
2446509.765861	0.944914	0.006519
2446509.766570	0.941808	0.006519
2446509.767278	0.950109	0.006519
2446509.767945	0.948028	0.006519
2446509.768653	0.965839	0.006519
2446509.769361	0.951151	0.006519
2446509.770028	0.953238	0.006519
2446509.770736	0.961623	0.006519
2446509.771445	0.961623	0.006519
2446509.772028	0.962676	0.006519
2446509.784611	0.995790	0.006519
2446509.785320	1.007770	0.006519
2446509.786028	1.022085	0.006519
2446509.786695	1.012156	0.006519
2446509.787403	1.015456	0.006519
2446509.788111	1.012156	0.006519
2446509.788778	1.015456	0.006519
2446509.789486	1.013255	0.006519
2446509.790195	1.013255	0.006519
2446509.790861	1.022085	0.006519
2446509.791570	1.026524	0.006519
2446509.792278	1.018766	0.006519
2446509.792945	1.016559	0.006519
2446509.793653	1.019871	0.006519
2446509.794361	1.007770	0.006519
2446509.795736	1.028749	0.006519
2446509.796445	1.008865	0.006519
2446509.799445	1.011058	0.006519
2446509.800153	1.001220	0.006519
2446509.801403	1.001220	0.006519
2446509.802695	1.018766	0.006519
2446509.803361	1.004491	0.006519
2446509.804070	1.005583	0.006519
2446509.805445	1.000132	0.006519
2446509.807528	1.018766	0.006519
2446509.808236	1.009961	0.006519
2446509.808945	1.006676	0.006519
2446509.809611	1.004491	0.006519
2446509.810320	1.017662	0.006519

22 May 87

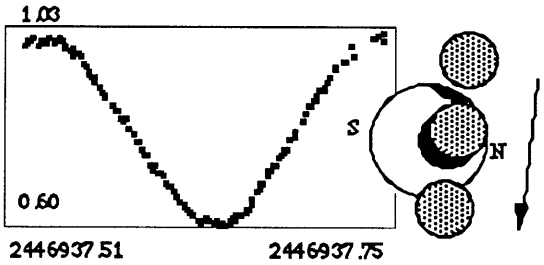

Julian Date	Normalized Intensity	± Sigma
2446937.522037	0.986957	0.005756
2446937.523195	0.999390	0.005756
2446937.524354	0.996351	0.007928
2446937.525512	0.999064	0.005756

2446937.526670	1.006913	0.005756
2446937.530604	0.990511	0.005756
2446937.531991	0.999716	0.005756
2446937.533033	0.992671	0.006190
2446937.534308	0.998955	0.005756
2446937.535466	0.995267	0.005756
2446937.536620	1.006148	0.005647
2446937.539400	0.992563	0.005756
2446937.540558	0.999607	0.005756
2446937.541716	1.000586	0.005756
2446937.542870	1.002437	0.005756
2446937.544029	0.999607	0.005756
2446937.545187	1.002219	0.005756
2446937.546345	0.985990	0.005973
2446937.547504	0.981593	0.005756
2446937.550050	0.980202	0.005756
2446937.551204	0.983307	0.005756
2446937.552362	0.967865	0.005756
2446937.553520	0.971574	0.005756
2446937.554679	0.971043	0.005756
2446937.555837	0.964802	0.006625
2446937.558383	0.949606	0.005865
2446937.559537	0.945035	0.007168
2446937.560695	0.935434	0.005865
2446937.561854	0.926017	0.006516
2446937.563012	0.920324	0.005865
2446937.564170	0.919918	0.007385
2446937.565325	0.911336	0.005973
2446937.568337	0.901723	0.005973
2446937.569491	0.887561	0.006082
2446937.570650	0.879231	0.006082
2446937.571808	0.883927	0.006082
2446937.576670	0.861709	0.006190
2446937.577825	0.853485	0.006190
2446937.578983	0.848260	0.006190
2446937.581529	0.834143	0.006190
2446937.582687	0.828365	0.007168
2446937.583845	0.835827	0.006190
2446937.585004	0.832462	0.006190
2446937.586158	0.812049	0.006299
2446937.588937	0.798790	0.006408
2446937.590095	0.787222	0.006408
2446937.591254	0.784107	0.006408
2446937.592408	0.785707	0.006408
2446937.593566	0.768332	0.006516
2446937.596345	0.758247	0.006516
2446937.597504	0.755915	0.007494
2446937.598658	0.734596	0.006625
2446937.599816	0.722788	0.006734
2446937.602595	0.733754	0.006625
2446937.603754	0.720710	0.006734
2446937.604908	0.716568	0.006734
2446937.606066	0.717643	0.006734
2446937.607225	0.713763	0.006734
2446937.608383	0.697600	0.008037
2446937.610929	0.689789	0.007168
2446937.612087	0.688507	0.006842
2446937.613241	0.680460	0.008906
2446937.614400	0.677609	0.006842
2446937.615558	0.671623	0.006842
2446937.616716	0.660006	0.006951
2446937.619491	0.653989	0.006951
2446937.620650	0.648625	0.007059
2446937.621808	0.638680	0.007277
2446937.622966	0.634765	0.007059
2446937.624120	0.637624	0.007059
2446937.625279	0.631393	0.007168
2446937.628287	0.620399	0.008580
2446937.629445	0.615324	0.007277
2446937.630604	0.614152	0.007277
2446937.631762	0.620251	0.007277
2446937.632920	0.623503	0.007168
2446937.634075	0.617968	0.007277
2446937.635233	0.619072	0.007277
2446937.637779	0.615617	0.007277
2446937.638937	0.615324	0.007277
2446937.640095	0.620325	0.007277
2446937.641254	0.609918	0.007385
2446937.642408	0.614518	0.007277
2446937.643566	0.611740	0.007385
2446937.644608	0.609626	0.008037
2446937.647270	0.612178	0.007385
2446937.648429	0.618851	0.007385
2446937.649587	0.623800	0.007277
2446937.650741	0.621358	0.007385
2446937.651900	0.629600	0.007277
2446937.653058	0.629152	0.007385
2446937.654216	0.631019	0.007385
2446937.656991	0.637473	0.007385
2446937.658150	0.641325	0.007277
2446937.659308	0.640190	0.007385
2446937.660466	0.650690	0.007277
2446937.661620	0.662177	0.007277
2446937.664400	0.682365	0.007168
2446937.665558	0.687147	0.007168
2446937.666716	0.695177	0.007168
2446937.667870	0.697115	0.007168
2446937.670420	0.712857	0.007059
2446937.671575	0.724954	0.007059
2446937.672733	0.726373	0.007059
2446937.673891	0.735102	0.006951
2446937.675050	0.735946	0.006951
2446937.677825	0.752643	0.006951
2446937.678983	0.754450	0.006951
2446937.680141	0.764320	0.006842
2446937.681300	0.768681	0.006842
2446937.682454	0.770519	0.006842
2446937.683612	0.790794	0.006734
2446937.686391	0.795997	0.006734
2446937.687550	0.807488	0.006951
2446937.692408	0.829294	0.006625
2446937.693566	0.843155	0.006625
2446937.696112	0.860366	0.006625
2446937.697270	0.864593	0.007168
2446937.698429	0.874653	0.006625
2446937.699587	0.872614	0.006625
2446937.700741	0.883829	0.006625
2446937.701900	0.894174	0.006625

2446937.704679	0.897147	0.006625
2446937.705837	0.901325	0.006734
2446937.706991	0.911738	0.006734
2446937.708150	0.924184	0.006734
2446937.711158	0.936463	0.006842
2446937.712316	0.944724	0.006842
2446937.716483	0.955451	0.005539
2446937.717641	0.956393	0.005647
2446937.721575	0.989002	0.005647
2446937.722733	0.966808	0.005756
2446937.723658	0.964485	0.008037
2446937.734770	1.006694	0.005973
2446937.735929	1.003091	0.007820
2446937.737087	1.008774	0.006842
2446937.740325	1.017460	0.006190
2446937.741483	0.999281	0.007820

18 Apr 88

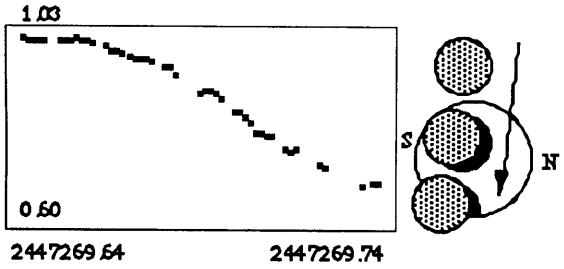

Julian Date	Normalized Intensity	± Sigma
2447269.644640	1.004480	0.004454
2447269.646027	0.999035	0.004454
2447269.647415	1.002190	0.004454
2447269.648807	0.998926	0.004454
2447269.650194	0.997623	0.004454
2447269.653898	1.000013	0.006083
2447269.655286	0.997732	0.004454
2447269.656677	0.998492	0.004454
2447269.658065	1.003607	0.005649
2447269.659453	1.001646	0.004345
2447269.660844	0.997623	0.005214
2447269.661998	0.993831	0.005432
2447269.665702	0.990375	0.004454
2447269.667094	0.978144	0.006083
2447269.668482	0.979746	0.004454
2447269.669869	0.969425	0.004454
2447269.671723	0.965512	0.004454
2447269.673111	0.958357	0.004563
2447269.674498	0.963614	0.005432
2447269.675890	0.959931	0.004780
2447269.677277	0.958042	0.006192
2447269.680519	0.943971	0.004563
2447269.681907	0.942936	0.004563
2447269.683298	0.927826	0.004563
2447269.689315	0.891181	0.004780
2447269.690703	0.893257	0.004780
2447269.692094	0.893257	0.004780
2447269.693482	0.891478	0.004780
2447269.694869	0.878132	0.004780
2447269.697882	0.850132	0.004888
2447269.699269	0.851082	0.004888
2447269.700657	0.841905	0.004888
2447269.702044	0.829456	0.004997
2447269.703436	0.806009	0.007170
2447269.704823	0.807646	0.005106
2447269.706215	0.803830	0.005214
2447269.707602	0.802743	0.005106
2447269.711307	0.772162	0.012819
2447269.712694	0.767347	0.005214
2447269.714082	0.774710	0.005214
2447269.719640	0.741427	0.006518
2447269.721027	0.736177	0.005540
2447269.730519	0.696285	0.011515
2447269.733294	0.699279	0.007713
2447269.734686	0.702201	0.009234

30 Apr 89

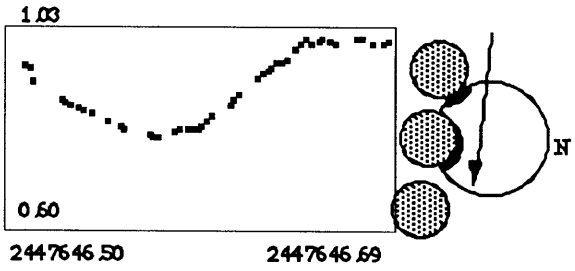

Julian Date	Normalized Intensity	± Sigma
2447646.509525	0.952130	0.004460
2447646.511837	0.943917	0.004243
2447646.514154	0.918826	0.003481
2447646.527346	0.876133	0.003916
2447646.529663	0.872829	0.003481
2447646.531975	0.867506	0.003481
2447646.536142	0.863555	0.003372
2447646.538458	0.858566	0.003372
2447646.542162	0.848754	0.004678
2447646.550262	0.832295	0.003372
2447646.555821	0.825600	0.003372
2447646.558133	0.816283	0.003481
2447646.569942	0.805053	0.003372
2447646.572254	0.799711	0.005875
2447646.574571	0.803330	0.003372
2447646.582442	0.814907	0.003372
2447646.584175	0.817845	0.004787
2447646.588692	0.819318	0.004134

2447646.591004	0.817662	0.003372
2447646.593321	0.815733	0.004678
2447646.595633	0.825971	0.003372
2447646.597950	0.834630	0.003481
2447646.600263	0.843836	0.006636
2447646.608596	0.867892	0.003264
2447646.610913	0.876815	0.003590
2447646.613225	0.891130	0.003372
2447646.622254	0.922985	0.003046
2447646.624571	0.934326	0.003046
2447646.626883	0.936999	0.003046
2447646.629200	0.944954	0.003481
2447646.631513	0.957778	0.003046
2447646.633829	0.955369	0.003046
2447646.636029	0.962716	0.003155
2447646.640542	0.983437	0.002937
2447646.642858	0.995290	0.002937
2447646.645171	1.003551	0.003372
2447646.647487	0.996916	0.002937
2447646.651654	0.998979	0.002937
2447646.653738	1.005406	0.004787
2447646.657442	0.999848	0.002937
2447646.659408	0.996808	0.005766
2447646.670171	1.007374	0.002937
2447646.672487	1.003987	0.002937
2447646.678275	0.996482	0.004243
2447646.682904	0.994532	0.003699
2447646.685217	1.000827	0.002937

24 Feb 90

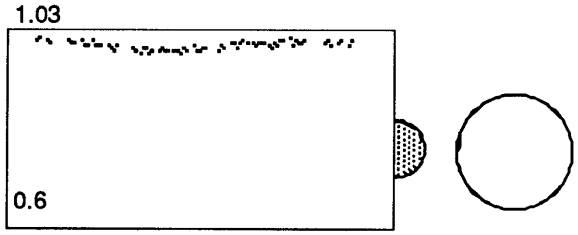

Julian Date	Normalized Intensity	± Sigma
2447946.695506	1.006448	0.006097
2447946.696665	1.009075	0.004573
2447946.700598	1.003826	0.005661
2447946.701756	0.998819	0.004573
2447946.709165	1.004590	0.005335
2447946.710323	0.997082	0.004464
2447946.711477	1.001538	0.004464
2447946.714490	1.004481	0.005553
2447946.715644	0.990915	0.005117
2447946.716802	0.994157	0.004464
2447946.719810	1.002082	0.005117
2447946.720969	0.991131	0.004464
2447946.722127	0.994698	0.004464
2447946.723285	0.994806	0.004790
2447946.726060	0.993508	0.004464
2447946.727219	0.989513	0.004355
2447946.728377	0.980281	0.005117
2447946.729536	0.991023	0.005226
2447946.735786	0.990376	0.004355
2447946.736944	0.983493	0.004355
2447946.739952	0.978999	0.004355
2447946.741111	0.988005	0.004355
2447946.742265	0.984781	0.005226
2447946.743423	0.978465	0.004899
2447946.744581	0.980709	0.005117
2447946.747361	0.983922	0.004355
2447946.748515	0.984996	0.005226
2447946.749673	0.980174	0.004355
2447946.750831	0.979533	0.008165
2447946.753606	0.979106	0.004355
2447946.754765	0.982957	0.004246
2447946.755923	0.982529	0.004246
2447946.757081	0.978358	0.004246
2447946.758240	0.986715	0.004246
2447946.759394	0.984352	0.004464
2447946.762173	0.991239	0.006750
2447946.763331	0.984673	0.004246
2447946.764490	0.982208	0.004246
2447946.765644	0.990052	0.004246
2447946.766802	0.985210	0.004246
2447946.772590	0.984030	0.004246
2447946.773748	0.993508	0.004246
2447946.774906	0.988651	0.005988
2447946.777681	0.999362	0.004137
2447946.778840	0.996973	0.006968
2447946.779998	0.989621	0.004246
2447946.781156	0.997407	0.004137
2447946.782310	1.006885	0.005008
2447946.785323	0.999145	0.004137
2447946.786477	1.000776	0.004137
2447946.787636	0.993075	0.004246
2447946.788794	0.997299	0.004464
2447946.789952	1.000232	0.004137
2447946.791106	0.998819	0.004137
2447946.793885	0.994373	0.004137
2447946.795044	0.990160	0.004137
2447946.796202	0.999688	0.004137
2447946.797356	0.993400	0.004137
2447946.798515	1.002191	0.004464
2447946.799673	1.006666	0.004137
2447946.802452	1.007541	0.004573
2447946.803611	0.992211	0.005879
2447946.804765	1.003826	0.004790
2447946.805923	1.000776	0.004137
2447946.807081	0.996973	0.004790
2447946.808240	1.003717	0.005008
2447946.817727	1.001320	0.004790
2447946.818886	1.002845	0.004137
2447946.819927	0.992211	0.004682
2447946.822590	0.999906	0.004573
2447946.823748	1.003608	0.005226
2447946.828144	0.995673	0.004246
2447946.829302	1.002191	0.004790

Appendix B

The Fitting Procedure

In this analysis of the mutual occultation lightcurves we have used the simplest albedo model possible; namely, we let the brightness of Pluto be the sum of the panel reflectivities times their respective projected areas. The advantage of such a simple model is clear: since it depends linearly on the parameters, a least squares fitting routine will find the best fit parameters on the first iteration. A model that incorporates limb darkening or phase reflectivity is nonlinear and does not have this advantage.

The best description of the least squares fitting procedure is in section 14.3 of *Numerical Recipes* (either C or Fortran versions) [Press et al 1988]. An overview of that material is presented here.

According to our model, Pluto's reflected intensity is the sum of the intensities from the panels[10]. Each panel's intensity is the product of its area (which is a function of time) and its reflectivity.

$$I(t) = \sum_{k=1}^{n} r_k A_k(t)$$

Equation B.1
I(t) is the model's prediction for the total amount of light from Pluto at time t, r is the reflectivity (or albedo) of the kth panel, and A(t) is the exposed area of the kth panel at time t. There are n panels. In our model the units of I(t) and A(t) are normalized to 1.0 for the entire disk. That is, a panel that covered half of Pluto's disk at time t would have a value of A(t) = 0.5.

We define a quantity, χ^2 (chi square), to indicate the quality of a fit.

$$\chi^2 = \sum_{i=1}^{N} \left[\frac{y(t_i) - I(t_i)}{\sigma_i} \right]^2$$

Equation B.2
This equation is called the *Merit Function*. y(t) is the observed light from Pluto at time t. N is the number of data points. σ is the standard deviation of the ith measurement. In this paper we assume that all of the measurements have the same weight, so the σ's always equal 1[11].

Minimization of χ^2 is done in the usual way; by setting the derivatives of χ^2 with respect to the parameters (the n panel albedos) equal to zero. After some manipulation, we get the matrix equation

$$[\alpha]\,\bar{a} = \bar{\beta}$$

Equation B.3
These are the *Normal Equations*. The matrix [α] is the inverse of the covariance matrix, $\bar{a}$ is the vector of least

10. The raw data sets include Charon's contribution too, of course. We have subtracted a constant representing Charon's contribution from every data point.

11. We have two ways of estimating the rms noise level of an observed data point. First, data point is usually a boxcar average of a number of points, so we estimate the noise from the fluctuations within the boxcar. Second, we expect that the signal is a Poisson distributed variable. The rms noise of such a variable is the square root of the variable's mean value. We choose whichever estimate is higher.

squares solutions for the n panel albedos (i.e., the answers), and $\underline{\beta}$ depends on the observed data.

$$A = \begin{bmatrix} \frac{A_1(t_1)}{\sigma_1} & \frac{A_2(t_1)}{\sigma_1} & \cdots & \frac{A_n(t_1)}{\sigma_1} \\ \frac{A_1(t_2)}{\sigma_2} & \frac{A_2(t_2)}{\sigma_2} & \cdots & \frac{A_n(t_2)}{\sigma_2} \\ \\ \\ \frac{A_1(t_N)}{\sigma_N} & \frac{A_2(t_N)}{\sigma_N} & \cdots & \frac{A_n(t_N)}{\sigma_N} \end{bmatrix}$$

Equation B.4
[A] is the *design matrix* for the least squares problem in which there are n parameters to fit and N data points. In our case, the elements of [A] are the n panel areas, evaluated at each of the N observation times.

$$[\alpha] = \mathbf{A}^T \mathbf{A}$$

or

$$\alpha_{kj} = \sum_{i=1}^{N} \frac{A_j(t_i)\, A_k(t_i)}{\sigma_i^2}$$

and

$$[\beta] = \frac{\mathbf{A}^T y}{\sigma_i^2}$$

or

$$\beta_k = \sum_{i=1}^{N} \frac{y(t_i)\, A_k(t_i)}{\sigma_i^2}$$

Equations B.5
[A] is the *design matrix* for the least squares problem in which there are n parameters to fit and N data points. In our case, the elements of [A] are the n panel areas, evaluated at each of the N observation times. Both [α] and $\underline{\beta}$ from equation B.3 can be written succinctly in terms of [A].

We can calculate the least squares solution, $\underline{a}$, with a single matrix inversion of [α], an n x n matrix.

There is a pitfall with regard to the uniqueness of the solution, however. If two or more parameters are very closely correlated, or the data set does not provide enough information to distinguish between them, then the matrix [α] will be nearly singular and will yield nonsense when we try to invert it.

As an example of how this might occur, consider the following transit of Pluto by Charon.

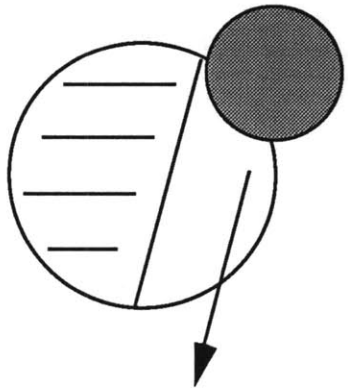

Figure B.1
In this example, suppose we only have data from a single transit, so that only right side of Pluto is covered by Charon. We would have problems if we split up the left side of Pluto into several panels, because there would be no way to distinguish between the contributions of the different panels from the data of this single transit.

Since Charon's passage does not cover the left part of Pluto, we would have no way of differentiating between any panels we might place there. The normal equations for any such panels would be linearly dependent, and we would not be able to invert the $[\alpha]$ matrix.

We use singular value decomposition (SVD) to deal with this possibility. The SVD tells us when we have pairs of parameters that are impossible to distinguish as well as finding the solution (out of all the non-unique solutions) that minimizes the residual, $[\alpha]\,\bar{a} - \bar{\beta}$. Of course, although we may get a solution that fits the data in such a case, we should certainly rework our choice of parameters. The SVD of an N x n matrix represents that matrix as the product of three matrices.

$$\mathbf{A} = [\mathrm{U}][\mathrm{V}][\mathrm{W}]$$

or

$$A = \underset{N \times n}{\begin{bmatrix} U \end{bmatrix}} \underset{\substack{\text{diagonal} \\ n \times n}}{\begin{bmatrix} W \end{bmatrix}} \underset{n \times n}{\begin{bmatrix} V \end{bmatrix}}$$

$$\begin{bmatrix} w & & & \\ & w & & \\ & & \cdots & \\ & & & w \end{bmatrix}$$

Equation B.6
The singular value decomposition of [A].

What good is this decomposition? It yields the least squares parameters in the following relation.

$$\bar{a} = \sum_{i=1}^{n} \frac{U_{(i)} y(t_i)}{w_i} V_{(i)}$$

Equation B.7
The least square parameter values from the SVD matrices.

In equation B.7 U(i) are the columns of [U] and V(i) are the rows of [V]. We see that the solutions to the least squares problem are "linear combinations of [V], with coefficients obtained by forming dot products of the columns of [U] with the weighted data vector." [Press et al 1988]. If a singular value, w, is zero, then equation B.7 will blow up, hardly more useful than the solution by the normal equations. The advantage of the SVD method is that we can edit the [W] matrix before using equation B.7. If an element of [W] is zero or very small, we should: (a) replace its reciprocal by zero, and (b) probably choose new parameters. Why do we replace the reciprocals of very small w's with zero?

> It may seem paradoxical ..., since zeroing a singular value corresponds to throwing away one linear combination of the set of equations that we are trying to solve. The resolution of the paradox is that we are throwing away precisely a combination of equations that is so corrupted by roundoff error as to be at best useless; usually it is worse than useless since it "pulls" the solution vector way off towards infinity along some direction that is almost a nullspace vector. In doing this, it compounds the roundoff problem and makes the residual |Ax - b| larger.[Press et al 1988]

So SVD is the method of choice. We check the condition number from the [W] matrix (the ratio of the largest w to the smallest one). The condition number should be a reasonable size, as opposed to 10^{12} or infinity.

Verification of the SVD Procedure

We have checked the SVD method on an artificial data set. Below is an illustration of the 21 panel 'Pluto' and the four panel 'Charon' used in the simulation.

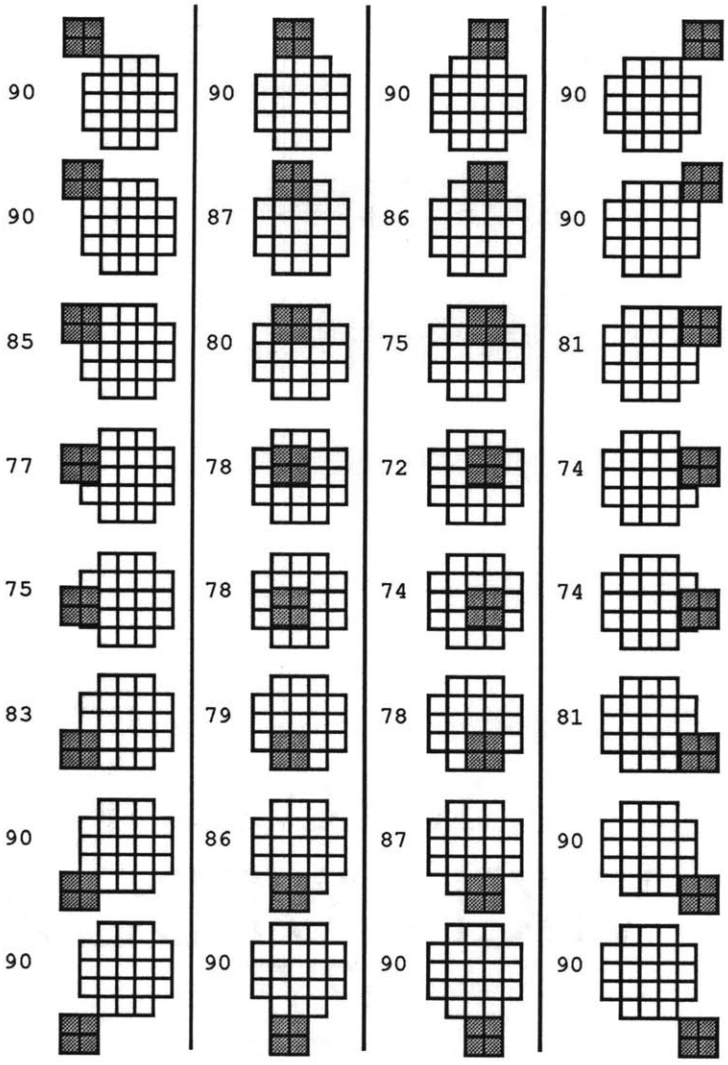

Figure B.2
The artificial data set used to test the SVD method. The observed intensity, minus Charon's contribution, is written next to each observation. There are 32 observations and 21 parameters to fit.

The normal least squares method could not solve for the panel albedos. We thought that the middle three rows might not be uniquely determined from this data set, and the SVD confirmed this. We added another strip of artificial observations, and found that both methods could solve for the panel brightnesses.

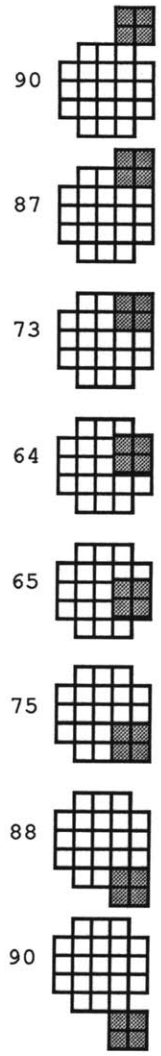

Figure B.3
This additional strip of data allowed both the SVD method and the normal method to solve for the panel brightnesses.

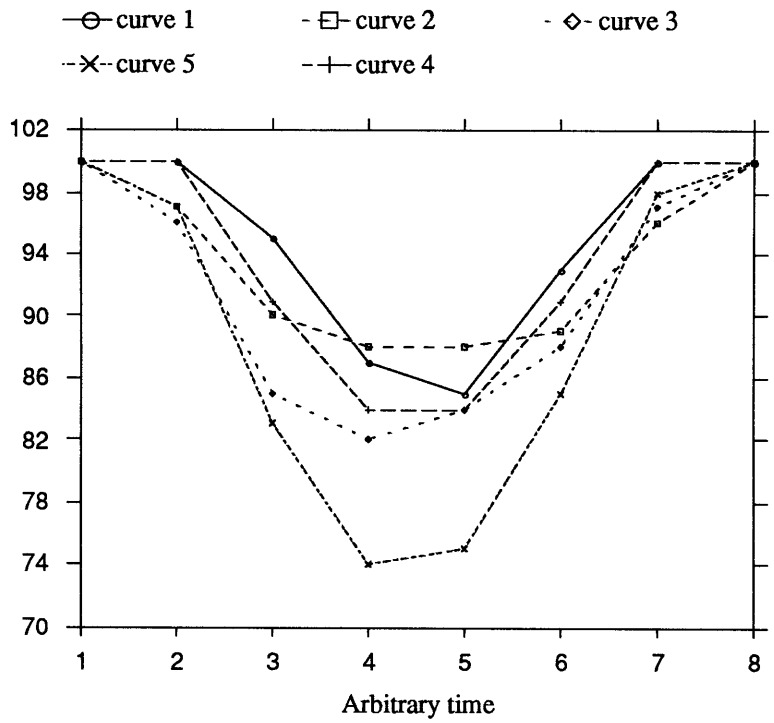

Figure B.4
The 5 artificial lightcurves.

We indexed the panels as follows.

	1	2	3	
4	5	6	7	8
9	10	11	12	13
14	15	16	17	18
	19	20	21	

Figure B.5
Numbers of the panels (for bookkeeping only).

The results of the SVD procedure with and without the fifth strip of data show that the problem is not unique without the fifth strip of data.

Panel number	non-unique sol'n	w's	unique sol'n	w's
1	1.666667	24.003	2	26.7337
2	1.333333	3	1	3.1668
3	2.666667	2.6259	3	2.9093
4	5	2.2889	5	2.6622
5	2	1.9319	1	2.4216
6	5	0.4293	6	2.2446
7	6	0.5176	5	1.9474
8	9	1	9	1.7495
9	8	0.9236	8	1.6434

10	2	0.8124	3	1.8413
11	3	1.7321	2	1.1954
12	4	1.8478	5	1.0824
13	7	1.7321	7	0.9559
14	7	0.7654	7	0.2088
15	2.666667	0	2	0.4088
16	4.333333	1.4142	5	0.5056
17	4.666667	1.4142	4	0.7875
18	9	1.4142	9	0.6993
19	2.666667	0	3	0.648
20	1.333333	0	1	0.6086
21	1.666667	0	2	1.4142

Table B.1
Results of the SVD procedure for the underdetermined and overdetermined data sets. The condition number for the underdetermined set is infinity, for the overdetermined set, 43.927.

Notice two things from this test: first, some w's are zero in the non-unique case, but the condition number is small in the unique case, and second, the SVD method found a solution in the non-unique case that minimized the residual, but was not the actual solution.

The solution from the normal equations (using Gaussian elimination to invert the matrix) gives the same results as the SVD method when all 40 observations are used.

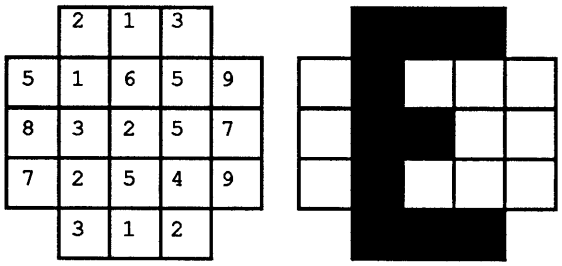

Figure B.6
The surface of the simulated planet was constructed in secret and had special significance. Only by solving the least squares problem and using the appropriate gray scale mapping could we verify that the solution was indeed correct.

Appendix C

The Orbital Geometry

Each object has six orbital elements:

a = semimajor axis

e = eccentricity

i = inclination

Ω = longitude of the ascending node

ω = argument of periapses

M = mean anomaly (associated with a particular time, or epoch)

The orbital elements for the Sun, Earth and Pluto came from the 1985 - 1989 editions of the Astronomical Almanac. We used Buie's and Tholen's determination of Charon's orbital elements (see table 1.1).

In a two body system the mean anomaly is the only coordinate that changes with time, which is the main advantage of the system of orbital elements. To convert from orbital elements to rectangular coordinates, one must first get the true anomaly from the mean anomaly, which requires solving Kepler's equation for the eccentric anomaly.

$$E - e \sin E = M$$

Equation C.1
Kepler's equation. E is the eccentric anomaly. This equation is the archetypal motivation for root finding algorithms[12].

The true anomaly, ν, is related to the eccentric anomaly by the relation

$$\tan\frac{\nu}{2} = \left[\frac{1+e}{1-e}\right]^{1/2} \tan\frac{E}{2}$$

Equation C.2

Once we have the true anomaly of the planet, the rectangular coordinates are given by

$$x = r\left\{\cos(\nu+\omega)\cos\Omega - \sin(\nu+\omega)\cos i \sin\Omega\right\}$$
$$y = r\left\{\cos(\nu+\omega)\sin\Omega - \sin(\nu+\omega)\cos i \cos\Omega\right\}$$
$$z = r \sin(\nu+\omega)\sin i$$

where r is the distance from the origin to the object

12. A reference for iterative solutions to Kepler's equation is R.H. Battin's book, *Astrodynamics* [Battin, R. H. 1987]. Our routine was originally written by Jim Klavetter.

$$r = \frac{a(1 - e^2)}{(1 + e \cos \nu)}$$

Equations C.3
x, y, and z related to the orbital elements of a planet[13].

We would like to rotate the coordinates of the Earth and Pluto from the frame of the ecliptic to the equatorial reference frame. This rotation requires a value for the obliquity, ε[14].

The equatorial coordinates are

$$\begin{aligned} x' &= x \\ y' &= y \cos \varepsilon - z \sin \varepsilon \\ z' &= y \sin \varepsilon + z \cos \varepsilon \end{aligned}$$

Equations C.4
The prime coordinates are in the equatorial reference frame, unprimed are in the ecliptic.

We still have to precess Charon's position from the J1950.0 frame to the J2000.0 frame. Theoretically we should be able to achieve this rotation by modifying just three of Charon's orbital elements prior to calculating its rectangular coordinates. The inclination, longitude of the ascending node, and the argument of pericenter are the only orbital elements affected by precession [Green, Robin M. 1985]. Unfortunately the formulae for updating these elements are too approximate for our use; contact times based on them would differ from the published predictions by over twenty minutes. We generated a more rigorous precession matrix to rotate Charon's position. Our contact time predictions are now always within two minutes, usually one, of Tholen and Buie's published contact times. The matrix we use to bring Charon from J1950 to J2000 coordinates is

$$P = \begin{bmatrix} 0.99992570859 & 0.01117889041 & 0.00485898322 \\ -0.01117889042 & 0.99993751388 & -0.0000271577 \\ -0.00485898319 & -0.00002716236 & 0.9999881947 \end{bmatrix}$$

Equation C.5
The matrix **P** rotates rectangular coordinates from a J1950 frame to J2000.0.

Pluto and Charon on the Projection Plane

We project Pluto and Charon onto a plane that is perpendicular to the line of sight from the Earth. To get the

13. Equations are from section **E** of the *Astronomical Almanac*, 1988 edition.
14. It turns out that the obliquity changes enough over the span of the data sets to require a time dependent formula (T is the time in Julian centuries after the epoch J2000.0, so T is negative until the second millenium):

$$\varepsilon = 23°26'21".448 - 46".815\ T - 0".001\ T^2 + 0".002\ T^3$$

positions of Pluto and Charon in this plane, we take the dot product of Pluto and Charon's position vectors with the two unit vectors that define the principal axes of the projection plane.

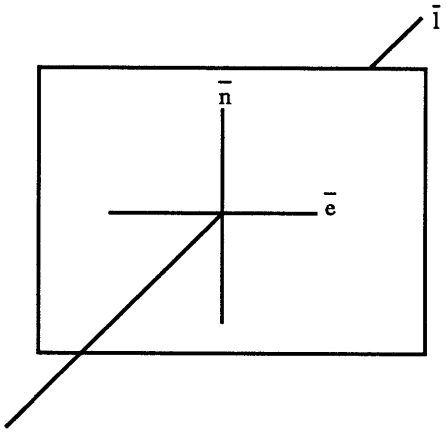

Figure C.1
The unit vector $\bar{l}$ points along the line of sight from the Earth, $\bar{n}$ points northward within the projection plane, and $\bar{e}$ points to the east.

How do we calculate the unit vectors $\bar{n}$ and $\bar{e}$? We know that $\bar{e}$ is perpendicular to the northward pointing unit vector, $\bar{z} = (0, 0, 1)$ and also perpendicular to $\bar{l}$, the line of sight unit vector. In fact, $\bar{e} = \bar{l} \times \bar{z}$. Once we have $\bar{e}$, we calculate $\bar{n}$ from the cross product $\bar{n} = \bar{e} \times \bar{l}$.

$$\bar{l} = \text{Pluto Coordinates} - \text{Earth Coordinates}$$

$$\bar{e} = \bar{l} \times \bar{z}$$

$$\bar{n} = \bar{e} \times \bar{l}$$

Equations C.6
These cross products give us the vectors $\bar{n}$ and $\bar{e}$, which define the projection plane. We generally will need to normalize $\bar{n}$ and $\bar{e}$.

The shadow of the Earthward body is cast upon the more distant body. We assume that the obstructing body leaves a cylinder of darkness behind it[15], so we represent the shadow with a disk the same size as the disk of the obstructing body.

15. The finite (and large) extent of the Sun creates a gray ring at the outer radius of the shadow called the penumbra. Since Pluto and Charon are so close to each other (20,000 km), the penumbra is only 6 km wide, insignificant compared to the scale of the current panel sizes.

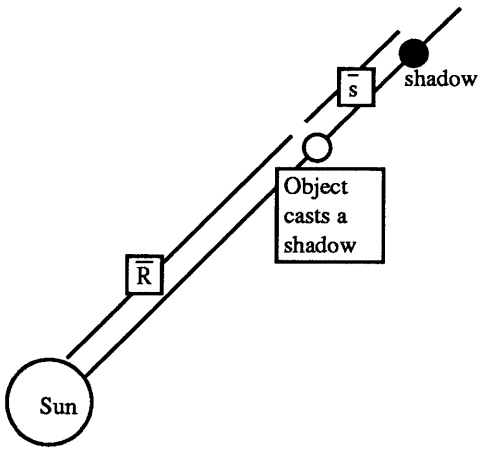

Figure C.2
The vector from the Sun to the Pluto-Charon system is $\overline{R}$. The shadow's offset from the obscuring body is $\overline{s}$, which is parallel to $\overline{R}$. The length of $\overline{s}$ is the separation between the body that casts the shadow and the surface upon which the shadow appears. In our case, the magnitude of $\overline{s}$ is the dot product of the Pluto-Charon separation vector and the unit vector which points in the $\overline{R}$ direction.

The separation between Pluto's surface and Charon's surface is, of course, affected by the curvatures of the two surfaces. In determining the shadow location we approximate the surface to surface distance with the distance between the two planet centers.

Appendix D

The Panel Map in Detail

Each panel is identified by five parameters: a central latitude and longitude, an extent in latitude and longitude, and an albedo. The panel coordinates refer to Pluto's local coordinate system. We need to know the position of the panel vertices on the projection plane. Each point of the panel's borders must be

- transformed to Plutocentric rectangular coordinates,
- rotated to the J2000.0 equatorial system,
- projected onto the projection plane.

How do we transform from Pluto's reference frame to the standard frame?

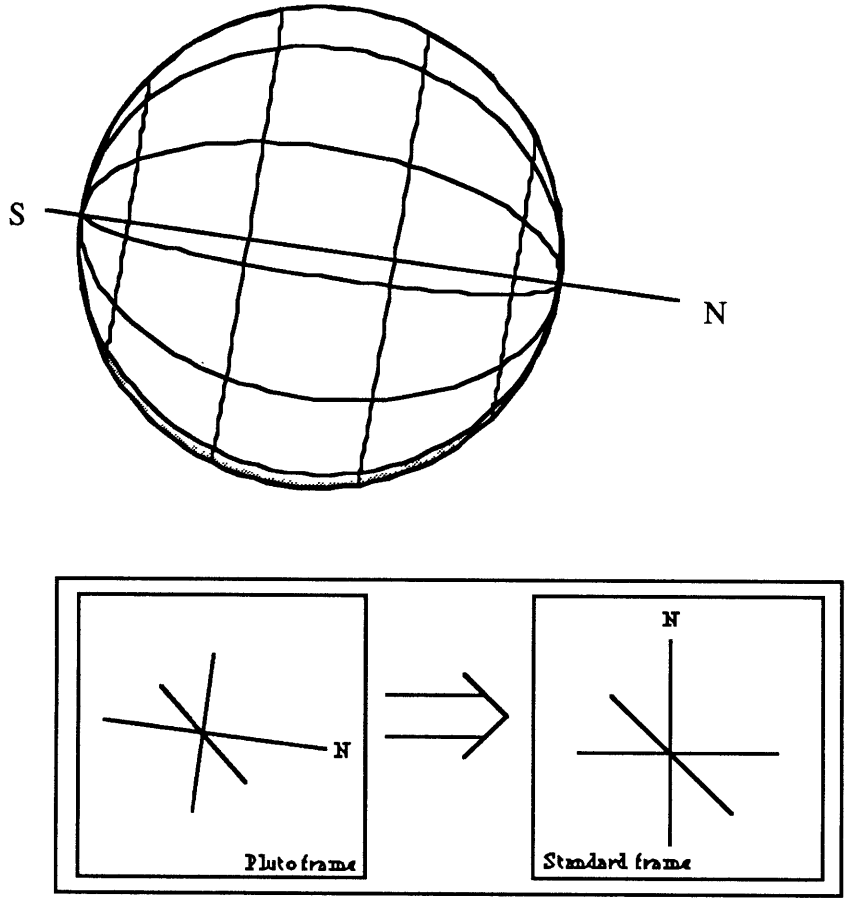

Figure D.1
What is the rotation matrix that transforms coordinates from the local Pluto reference frame to the standard frame?

The north pole of Pluto is defined by its spin and the right-hand convention. The choice of prime meridian is

more arbitrary. We have chosen the sub-Charon longitude as the prime meridian for Pluto, the same convention used by Buie and Tholen [Buie, M.W. and Tholen, D.J. 1988]. Because of the spin-orbit synchronicity, the location of the sub-Charon point should not move appreciably on Pluto's surface. The third rectangular coordinate is given by the cross product of the first two.

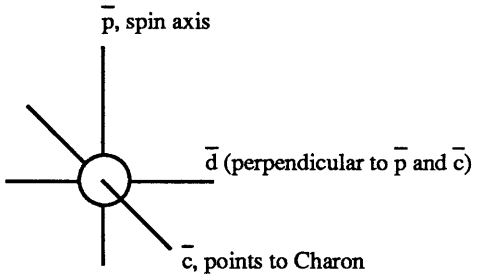

Figure D.2
The unit vectors that define the local Pluto frame. The direction of $\bar{d}$ is given by $\bar{p} \times \bar{c}$.

We want the matrix **R** that satisfies the following equations:

$$R\left[\bar{c}\right]=[1\ 0\ 0],$$
$$R\left[\bar{d}\right]=[0\ 1\ 0],$$
$$R\left[\bar{p}\right]=[0\ 0\ 1]$$

Equation D.1

The matrix is $\underline{R}=\left[[\bar{c}][\bar{d}][\bar{p}]\right]$ Equation D.2 [Young, L. A. 1989]

Curved v. Flat Panels

The panels are physically described by four parameters: a latitude and longitude of the panel center, and a panel height (extent in latitude) and width (extent in longitude).

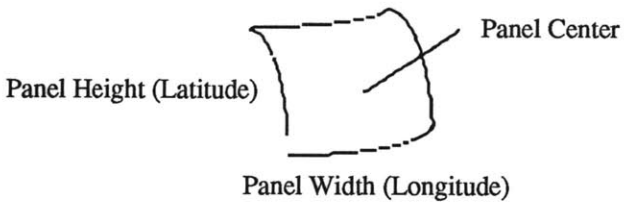

If we approximate the panels as being flat, the disk of Pluto loses area near the limb. The straight borders of the panels do not do a good job of representing the limb of Pluto. We use curved panels because of this shortcoming in the flat panel approximation.

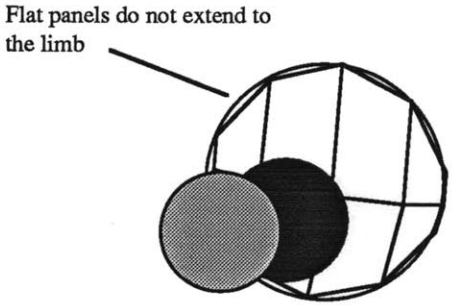

The curved panels have one problem that the flat panels do not; namely, the curved panels may curve around the limb, so that only a fraction of a panel is visible. A flat panel is either visible or hidden, but a curved panel may be partially visible. We need to be able to plot the limb if it passes though a panel.

Since Pluto's pole is nearly perpendicular to the line of sight from the Earth, the limb of Pluto will nearly coincide with a line of longitude in Pluto's local reference frame. Is the coincidence close enough for us to approximate the limb with a line of longitude? If the pole axis does not quite lie in the projection plane, then the projected lines of longitude will form ellipses within the circle of Pluto's limb.

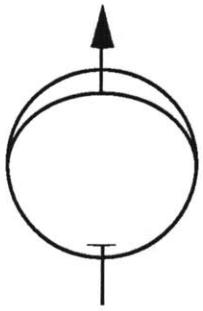

Suppose we find the line of longitude that best approximates the limb. How quickly will that line diverge from the limb? We need to know how tilted Pluto's pole is with respect to the projection plane. The more tilted Pluto's

pole, the thinner the ellipse formed by the projected lines of longitude. What is the worst-case tilt?

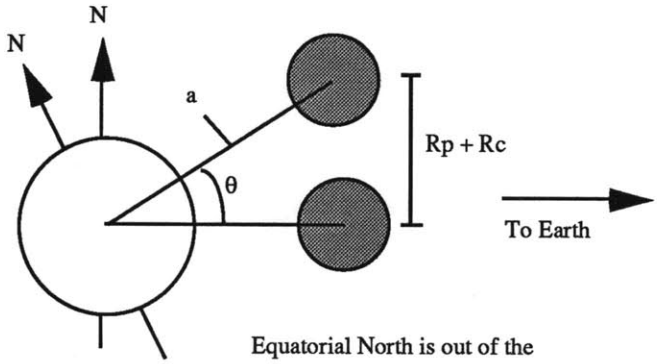

We see that the worst-case tilt is approximately given by

$$\sin(\theta) = (Rp + Rc) / a$$

(assuming that the Earth is so far away that the lines of sight to Pluto are essentially parallel).

If we plug in values of

a = 19640 km

Rp = 1142 km

Rc = 596 km

We get: $\theta = 5.07°$

Now we need to integrate to find the difference in projected areas between the limb and the line of longitude.

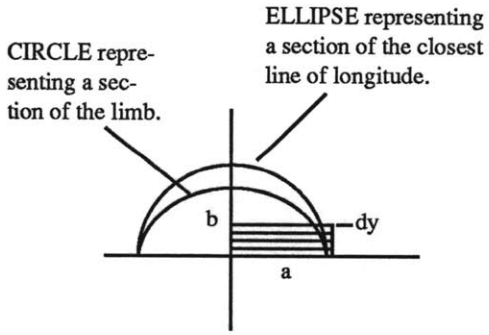

The semiminor axis is: $b = a \cos\theta = 0.996\ a$.

For the circle, each slice has an area of

$$d(\text{Area}) = x\,dy,$$
$$\text{where } x = a\sqrt{1 - \frac{y^2}{a^2}}$$

For the ellipse, each slice has an area of

$$d(\text{Area}) = x\,dy,$$
$$\text{where } x = a\sqrt{1 - \frac{y^2}{b^2}}$$

The area difference along a section of the limb is given by the integral

$$\text{Area Diff.} = a\int_{y=0}^{y=y\text{top}} \left(\sqrt{1 - \frac{y^2}{a^2}} - \sqrt{1 - \frac{y^2}{b^2}}\right) dy$$

We use a trig substitutions for the two parts of the integral

$$\sin\theta = \frac{y}{a}, \text{ or } \sin\theta = \frac{y}{b}$$
$$\text{so } dy = a\cos\theta\,d\theta, \text{ or } dy = b\cos\theta\,d\theta$$

The integral becomes

$$\text{Area Diff.} = a^2\int_{\theta=0}^{\theta} (\cos\theta)\cos\theta\,d\theta - ab\int_{0}^{\psi} (\cos\psi)\cos\psi\,d\psi$$

Use a trig substitution

$$2\cos^2\theta = \cos 2\theta + 1$$

we find the sol'ns to these integrals:

$$\text{Area Diff.} = \frac{a^2}{2}\left[\theta + \frac{\sin 2\theta}{2}\right]_{\theta=0}^{\theta} - \frac{ab}{2}\left[\psi + \frac{\sin 2\psi}{2}\right]_{\psi=0}^{\psi}$$

Rewrite the bounds in terms of y

$$\text{Area Diff.} = \frac{a^2}{2}\left[\theta + \frac{\sin 2\theta}{2}\right]_{\theta = 0}^{\theta_{top} = \sin^{-1}\left(\frac{y_{top}}{a}\right)} - \frac{ab}{2}\left[\psi + \frac{\sin 2\psi}{2}\right]_{\psi = 0}^{\psi_{top} = \sin^{-1}\left(\frac{y_{top}}{b}\right)}$$

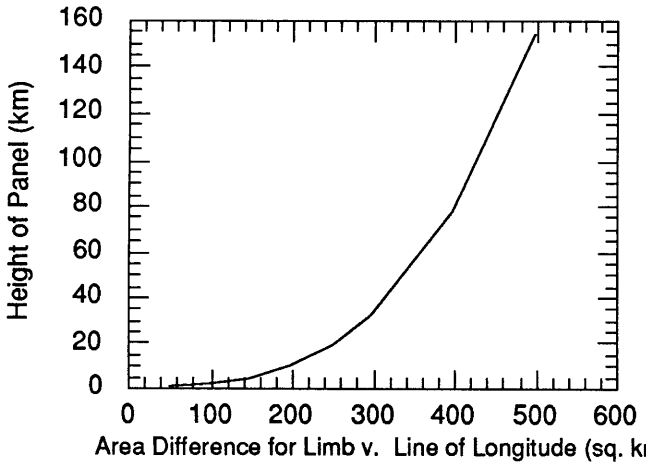

y top (km)	Area Diff.(sq km)
50	0.14
100	1.15
150	3.90
200	9.30
250	18.26
300	31.77
400	76.64
500	153.20

What are typical panel areas? Suppose we have split Pluto into 11 panels, each with a dimension of ~400 km. The panels near the equator will have an area of 164,000 sq km, so the error introduced by the limb approximation (76 sq km) is negligible.

Calculating the Exposed Area of a Panel

The exposed area of a panel is determined in a two step process. First we determine whether or not any part of a panel is obscured by Charon or its shadow. If the panel is not obscured, we calculate the projected area of the part of the panel which is on the viewer's hemisphere of Pluto. If the panel is obscured, then we subdivide the panel into a 30 x 30 grid. If an element of the grid is visible, we add its projected area to a cumulative total. The analytic expression for a panel is

$$\text{Area} = \frac{r^2}{2}\left[\begin{array}{c}\left(l_x\left(\sin\theta_f - \sin\theta_i\right) - l_y\left(\cos\theta_f - \cos\theta_i\right)\right)\left(\phi_f - \phi_i + \frac{\sin 2\phi_f - \sin 2\phi_i}{2}\right) \\ - l_z\left(\theta_f - \theta_i\right)\left(\cos 2\phi_f - \cos 2\phi_i\right)\end{array}\right]$$

Equation D.1 The projected area of a panel on Pluto in terms of the East-West bounds and the North-South bounds of the panel. NOTE: it is important that the line of sight vector, $\bar{l}$, be in the same coordinate system as the latitude and longitude variables θ and ϕ.

where r is the radius of Pluto, l_x, l_y, and l_z are components of the line of sight unit vector, $\bar{l}$, which points from the Sun to Pluto, θ_f, θ_i, ϕ_f and ϕ_i are the east, west, south and north bounds of the panel respectively. In practice we normalize panel areas so that Pluto's entire disk has an area of one (i.e., we divide by πr^2).

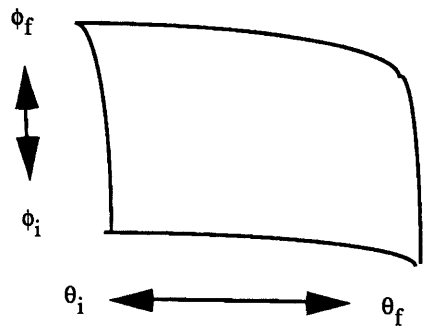

Figure D.4 The boundaries of a panel used in equation D.1.

When we calculate the panel areas by adding up elements of a grid, we need to determine the projected area of each element. We approximate each element as an infinitesimal surface unit. The projected area is

$$\Delta A = \frac{\Delta\lambda\,\Delta\phi}{\pi}\left(\cos^2\phi\left(l_x\cos\lambda + l_y\sin\lambda\right) + l_z\cos\phi\sin\phi\right)$$

Equation D.2 Area of an infinitesimal element.

where ΔA is the area of the element, λ and ϕ are the longitude and latitude of the element, and $\Delta\lambda$ and $\Delta\phi$ are the element's infinitesimal (or very small) extent in longitude and latitude.

We naturally compared the analytic method of panel area calculation with the 30 x 30 grid method. In all cases the area difference was less than one part in 4000.

When we implemented the Minnaert limb darkening law, we had to calculate all panel areas by the grid method. Each small area element not only had to be projected onto the projection plane (as is the case in equation D.2), but also had to be scaled by the limb darkening factor, which depended on the element's location on the disk. We checked the Minnaert model by running the model with k set to 0.5, and the results were identical to the ordinary, non-limb darkened case.

References

Aksnes, K. and Franklin, F.A. 1975. Mutual Phenomena of the Galilean Satellites in 1973. I. Total and Near-Total Occultations of Europa by Io. Astron. J. 80, 56-63.

Andersson, L.E. 1978. Eclipse Phenomena of Pluto and its Satellite. Bull. Amer. Astron. Soc. 10, 586.

Battin, R.H. 1987. An Introduction to the Mathematics and Methods of Astrodynamics. American Institute of Aeronautics and Astronautics, Inc., 1633 Broadway, New York, NY 10019

Beletic, J.W., Goody, R.M., and Tholen, D.J. 1989. Orbital Elements of Charon from Speckle Interferometry. Icarus 79, 38-46.

Binzel, R.P. 1988. Hemispherical Color Differences on Pluto and Charon. Science 241, 1070-1072.

Binzel, R.P. and Mulholland, J.D., 1984. Photometry of Pluto During the 1983 Opposition: A New Determmination of the Phase Coefficient. Astron. J. 89, 1759-1761.

Binzel, R.P., Tholen, D.J., Tedesco, E.F., Buratti, B.J., and Nelson, R.M., 1985. The Detection of Eclipses in the Pluto-Charon System. Science 228, 1193-1195.

Buie, M.W. and Tholen, D.J. 1988. The Surface Albedo Distribution of Pluto. Icarus 79 23-37.

Buie, M.W., 1984. Lightcurve CCD Spectrophotometry of Pluto. PhD. thesis, The University of Arizona, Tuscon, AZ.

Buie, M.W., Lebofsky, L.A., Tedesco, E.F. and Cruikshank, D.P. 1989. Methane Map of Pluto from Mutual Event Observations. B.A.A.S. 21, No. 3, 985.

Dobrovolskis, A.R., and Harris, A.W. 1983. The Obliquity of Pluto. Icarus 55, 231-235.

Dunbar, R.S. and Tedesco, E.F. 1986. Modeling Pluto-Charon Mutual Events. I. First Order Models. Submitted to the Astron. J.

Elliot, J.L., Dunham, E.W., Bosh, A.S., Slivan, S.M., Young, L.A., Wasserman, L.H., and Millis, R.L. 1989. Pluto's Atmosphere. Icarus 77, 148-170.

Elliot, J.L., Dunham, E.W., Veverka, J., and Goguen, J. 1978. Icarus 35, 237-246.

Green, R.M. 1985. Spherical Astronomy. Cambridge Unverstiy Press, Cambridge, England.

Horne, K., Buie, M.W. and Tholen, D.J. 1988. Maximum Entropy Maps of Pluto and Charon from Mutual Event Light Curves. Bull. Amer. Astron. Soc. 20, 1089.

Hoyt, W.G. 1980. Planets X and Pluto. The University of Arizona Press, Tuscon, AZ.

Marcialis, R.L. 1983. A Two Spot Model for the Surface of Pluto. Master's thesis, Vanderbilt University, Nashville, Tennessee.

Press, W.H., Flannery, B.P., Teukolsky, S.A. and Vetterling, W.T. 1988. Numerical Recipes in C. Press Syndicate of the University of Cambridge.

Sawyer, S.R., Reflectance Spectroscopy of the Surface and Atmosphere of Pluto-Charon. B.A.A.S. 21, 986.

Smith, B.A., Soderblom, L.A., Banfield, D., Barnet, C., Basilevsky, A.T., Beebe, R.F., Bollinger, K., Boyce, J.M., Brahic, A., Briggs, G.A., Brown, R.H., Chyba, C., Collins, S.A., Colvin, T., Cook II, A.F., Crisp, D.,

Croft, S.K., Cruikshank, D., Cuzzi, J.N., Danielson, G.E., Davies, M.E., De Jong, E., Dones, L., Godfrey, D., Goguen, J., Grenier, I., Haemmerle, V.R., Hammel, H., Hansen, C.J., Helfenstein, C.P., Howell, C., Hunt, G.E., Ingersoll, A.P., Johnson, T.V., Kargel, J., Kirk, R., Kuehn, D.I., Limaye, S., Masursky, H., McEwen, A., Morrison, D., Owen, T., Owen, W., Pollack, J.B., Porco, C.C., Rages, K., Rogers, P., Rudy, D., Sagan, C., Schwartz, J., Shoemaker, E.M., Showalter, M., Sicardy, B., Simonelli, D., Spencer, J., Sromovsky, L.A., Stoker, C., Strom, R.G., Suomi, V.E., Synott, S.P., Terrile, R.J., Thomas, P., Thompson, W.R., Verbiscer, A., Veverka, J. 1989. Science 246, 1422-1449.

Stern, S.A., Trafton, L.M. and Gladstone, G.R. 1988. Why is Pluto Bright? Implications of the Albedo and Lightcurve Behavior of Pluto. Icarus 75, 485-498.

Sykes, M.V., Cutri, R.M., Lebofsky, L.A. and Binzel, R.P. 1987. IRAS Serendipitous Survey Observations of Pluto and Charon. Science 237, 1336-1340.

Tholen, D.J. and Buie, M.W., 1989. Circumstances for Pluto-Charon Mutual Events in 1990. Astron. J.

Veverka, J. 1989. Conoco Lecture at the Massachusetts Institute of Technology.

Wild, W.J. 1989. Matrix Formalism for Inferring Planetary Surface Albedo Distributions from Light-Curve Measurements. Pub. Astron. Soc. Pac. 101, 844-848.